Characterization Of Motility Alterations Caused By The Impairment Of Dynein/dynactin Motor Protein Complex

2013

Swaran Nandini
University of Central Florida

CHARACTERIZATION OF MOTILITY ALTERATIONS CAUSED BY THE IMPAIRMENT OF DYNEIN/DYNACTIN MOTOR PROTEIN COMPLEX

by

SWARAN NANDINI
B.Tech. Jaypee Institute of Information Technology (India), 2011

A thesis submitted in partial fulfillment of the requirements
for the degree of Master of Science
in the Burnett School of Biomedical Sciences
in the College of Medicine
at the University of Central Florida
Orlando, Florida

Summer Term
2013

Major Professor: Stephen J. King

ABSTRACT

Transport of intracellular cargo is an important and dynamic process required for cell maintenance and survival. Dynein is the motor protein that carries organelles and vesicles from the cell periphery to the cell center along the microtubule network. Dynactin is a protein that activates dynein for this transport process. Together, dynein and dynactin forms a motor protein complex that is essential for transport processes in all the vertebrate cells. Using fluorescent microscope based live cell imaging techniques and kymograph analyses, I studied dynein/dynactin disruptions on the intracellular transport in two different cell systems. In one set of experiments, effects of dynein heavy chain (DHC) mutations on the vesicular motility were characterized in the fungus model system *Neurospora crassa.* I found that many DHC mutations had a severe transport defect, while one mutation linked to neurodegeneration in mice had a subtle effect on intracellular transport of vesicles. In a different set of experiments in mammalian tissue culture CAD cells, I studied the effects of dynactin knockdown and dynein inhibition on mitochondrial motility. My results indicated that reductions in dynactin levels decrease the average number of mitochondrial movements and surprisingly, increase the mitochondrial run lengths. Also, I determined that the dynein inhibitory drug Ciliobrevin causes changes in mitochondrial morphology and decreases the number of mitochondrial movements inside cells. Overall, my research shows that distinct disruptions in the dynein and dynactin motor complex alters intracellular motility, but in different ways. So far, my studies have set the ground work for future experiments to analyze the motility mechanism of motor proteins having mutations that lead to neurodegenerative disorders.

TABLE OF CONTENTS

LIST OF FIGURES vii

LIST OF TABLES ix

CHAPTER 1: INTRODUCTION 1

1.1 Role of the dynein-dynactin motor protein complex in transport 2

1.2 Role of the dynein-dynactin motor protein complex in cell maintenance 4

1.3 Dynein structure and function 4

1.3.1 Dynein heavy chain 6

1.4 Dynactin structure and function 7

1.5 Role of the dynein-dynactin motor protein complex in neurodegeneration 9

1.5.1 Neurodegeneration linked mutations in dynein 10

1.5.2 Neurodegeneration linked mutations in dynactin 11

1.6 Hypothesis: Dynein/dynactin motor protein complex and Neurodegeneration 12

CHAPTER 2: *N. crassa* MOTILITY ANALYSES 14

2.1 Introduction: *N.crassa* as a model system to study dynein function 14

2.2 Background work on *N. crassa* 14

2.2.1 The *ropy* mutants 14

2.2.2 Isolation of *N. crassa* DHC class mutants 16

2.2.3 Generation of *N. crassa Loa* mutants 20

2.3 Results and discussion 22

2.3.1 *N. crassa* DHC class mutants results 22

2.3.2 *N.crassa Loa* mutant results 29

2.4 Future directions 32

CHAPTER 3: CAD CELLS MOTILITY ANALYSES 33

3.1 Introduction 33

3.2 Rationale for the approach 33

3.3 Background work: p150 knockdown quantification 36

3.4 Results and discussion 41

3.4.1 Effects of dynactin disruption on motility 41

3.4.2 Effects of dynein inhibition on motility 46

3.5 Future directions 48

CHAPTER 4: MATERIALS AND METHODS 50

4.1 *N.crassa* motility analyses 50

4.1.1 Vesicle labeling 50

4.1.2 Live cell imaging 50

4.2 CAD cell motility analyses 51

4.2.1 Cell Culture 51

4.2.2 Transfection with knockdown plasmid 51

4.2.3 Mitochondria labeling 53

4.2.4 Ciliobrevin treatment..... 53

4.2.5 Live cell imaging..... 54

4.3 Kymograph and data analyses 55

REFERENCES 58

LIST OF FIGURES

Figure 1: Microtubule based cytoskeleton inside a cell 1

Figure 2: The dynein/dynactin motor complex 3

Figure 3: Dynein molecule structure 5

Figure 4: Dynein Heavy Chains (DHCs) structure 6

Figure 5: Dynactin molecule structure 8

Figure 6: The p150 subunit of dynactin 8

Figure 7: Neurodegenerative linked mutations in dynactin 12

Figure 8: The *ropy* mutants colony morphology 15

Figure 9: Isolation of *N. crassa* DHC class mutants 16

Figure 10: Comparison of DHC class mutant phenotypes 17

Figure 11: Localization of DHC class mutations 19

Figure 12: Tail suspension test 20

Figure 13: *Loa* tail mutation in *N. crassa* DHC 21

Figure 14: Localization of dynein in the mutant *Loa N. crassa* strain 22

Figure 15: Kymographs of the FM® 4-64 labeled vesicles in *N. crassa* hyphae 23

Figure 16: Kymographs of *N. crassa* mutant strains 24

Figure 17: Kymographs of the vesicles in the WT and mutant *Loa* hyphae 29

Figure 18: CAD cell in culture 33

Figure 19: p150 subunit 'knockdown and replacement' strategy in CAD cells 35

Figure 20: Other methods of disrupting dynactin function 35

Figure 21: Ciliobrevin inhibits dynein's motor activity 36

Figure 22: Immunostaining displaying p150 knockdown at 72 hrs 38

Figure 23: Quantification of p150 knockdown at 72 hrs 40

Figure 24: Kymographs of mitochondrial movements in CAD cells 41

Figure 25: Distance vs Velocity graph of mitochondrial movements 44

Figure 26: Histogram of percentage of mitochondrial movements 45

Figure 27: Effect of Ciliobrevin on mitochondrial motility 47

Figure 28: Knockdown sh-plasmid structure 51

Figure 29: Kymograph generation and analysis 56

LIST OF TABLES

Table 1: Comparison of motility parameters for the *N.crassa* WT and mutant strains 26

Table 2: Vesicle accumulation in *N. crassa* hyhae 26

Table 3: Comparison of motility parameters for the inward and the outward directed vesicular movements 27

Table 4: Summary of motility analysis of WT and *Loa* strains 30

Table 5: Mitochondrial motility data in CAD cells 42

CHAPTER 1: INTRODUCTION

Cells have to transport essential cargoes (such as organelles, vesicles, signal peptides, hormones) to maintain their health and to survive. Cytoskeletal motor proteins help in the transport of these cargoes using an extensive microtubule network inside the cell. The minus ends of the microtubule are capped near the MTOC and the plus end of microtubules extends outward towards the cell periphery (Fig. 1). Plus end directed motor proteins (kinesin) carry cargo from the cell center towards the cell periphery (Fig.1). In contrast, the minus end directed motor protein dynein carries cargo from the cell periphery to the cell center (Paschal and Vallee, 1987).

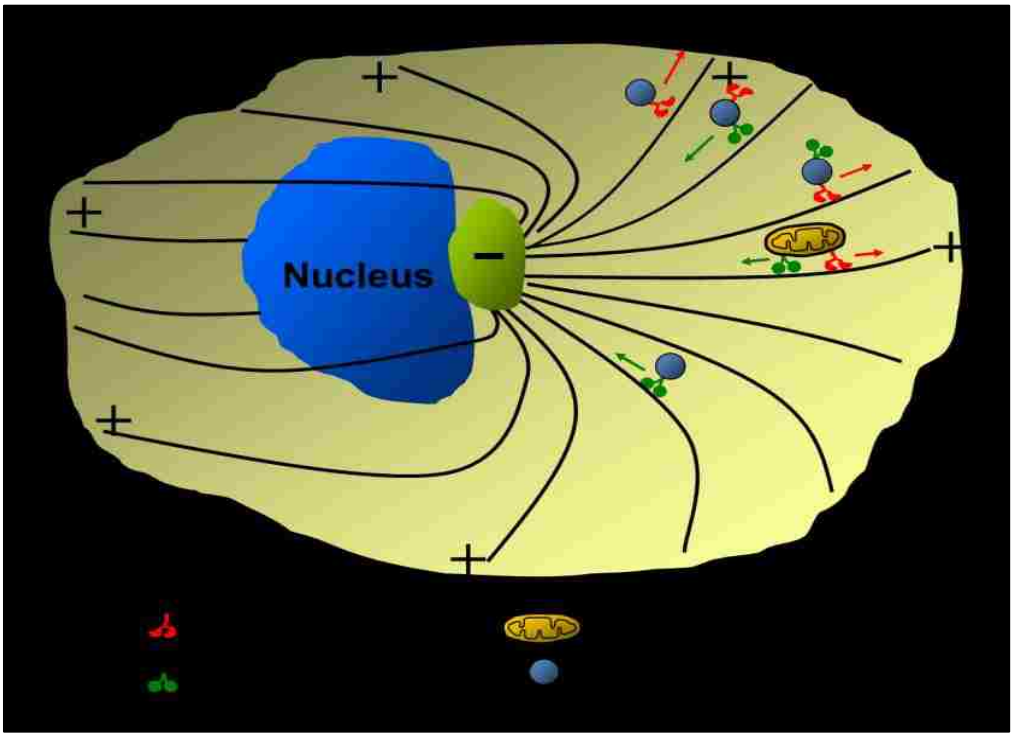

Figure 1: Microtubule based cytoskeleton inside a cell

Motor proteins (dynein and kinesin) carry cargo (blue vesicles) on a microtubule (MT) network inside a cell. The plus and minus signs denote the respective ends of MT. The arrows show the direction of the moving motor proteins.

A complicated system of motor protein involvement is needed to keep the robust transport system functioning inside cells. In some cases, a cargo might have two opposite motor proteins attached (Fig.1), of which only one motor protein (i.e. kinesin) can be active. In this case, the active kinesin carries the cargo towards the plus end of a microtubule. In the same cell, motor recycling happens that allows dynein to be recycled back to the plus end of the microtubule by kinesin. Consequently, dynein can bind to cargoes at the plus ends and carry them towards the minus ends of the microtubules. Other possibilities include having both kinesin and dynein active and attached on the same cargo (Fig.1, mitochondria shown). In such cases there could be a "tug-of-war" between the two opposite end directed motor proteins. Whichever motor protein manages to move can carry the cargo in the respective direction on the microtubule. For example, in the "tug-of-war" situation if dynein is active, then it will carry the cargo towards the minus end of the microtubule.

1.1 Role of the dynein-dynactin motor protein complex in transport

The motor protein dynein cleaves ATP and generates force to "walk" on the microtubule in a hand over hand fashion. During dynein's mechanochemical cycle, the ATP binds to the ATPase domains of dynein and gets hydrolyzed to ADP + P_i. The binding of ATP, its hydrolysis, and the subsequent release of products cause subsequent conformational changes in the dynein molecule. During this cycle, dynein's microtubule binding stalk is thought to change angle with respect to the rest of the molecule, which makes the MT binding stalks release or bind the microtubule (Gennerich and Vale, 2009). By taking sequential steps in the mechanochemical cycle, one head of the motor protein

takes a step forward and then binds to the next binding site on the microtubule. A dynein molecule alternates its globular heads while taking steps on the microtubule, as one of the heads has to maintain contact with the microtubule to avoid its accidental release into the cytoplasm. Ultimately, dynein does release both of its globular head from the microtubule to effectively terminate the transport event.

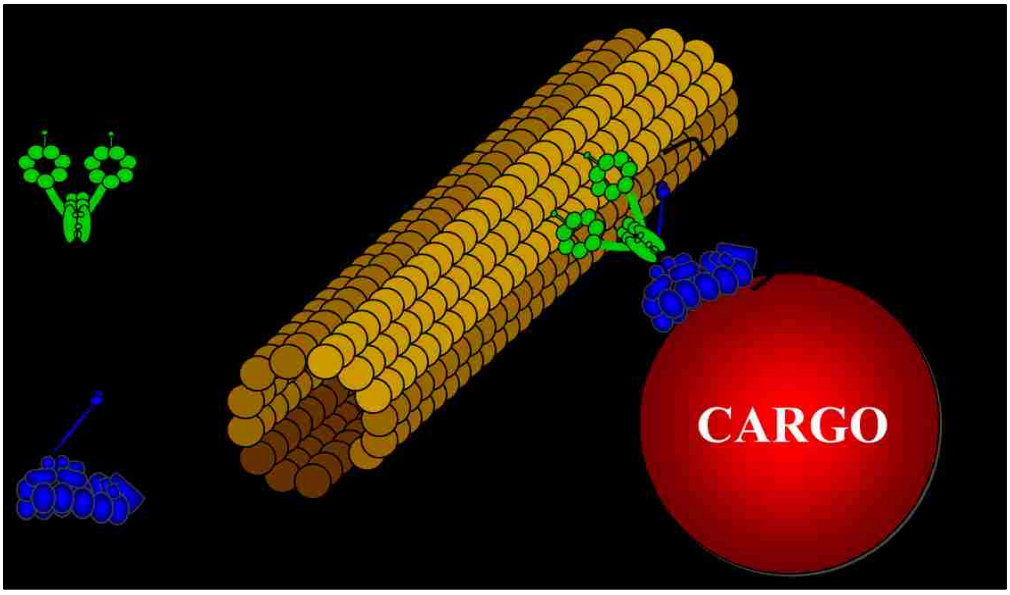

Figure 2: The dynein/dynactin motor complex

The model here shows how the dynein and dynactin molecules interact together to form a motor protein complex. This dynein/dynactin complex then carries the cargo on a microtubule, towards its minus ends. Dynactin helps in loading the cargo onto the dynein molecule by functioning as a cargo adaptor. Dynactin also maintains a contact with the microtubule by acting as a secondary linkage/molecular tether for the motor protein complex.

Dynein also interacts with its molecular activator dynactin (Fig.2) to form a motor protein complex. Dynactin acts a molecular tether (King and Schroer, 2000) to help dynein stay on the microtubule to continue the transport event in case dynein lets go of both of its globular heads. Hence, dynactin functions as a processivity factor (Culver-Hanlon et al., 2006) by helping dynein move a longer distance on the microtubule by

preventing its accidental diffusion into the cytoplasm. Recent studies show that mutations in dynactin inhibit the initiation of retrograde transport in neuronal axons (Lloyd et al., 2012). This suggests that dynactin also functions as a cargo adaptor for dynein and initiates transport events at the plus ends of the microtubule.

1.2 Role of the dynein-dynactin motor protein complex in cell maintenance

Together the dynein-dynactin motor complex plays an essential role in the intracellular transport. Total loss of dynein function causes early embryonic lethality in *Drosophila melanogaster* (Dick et al., 1996). Dynein-null mouse embryos lacking dynein do not survive to the gastrulation stage (Harada et al., 1998). The dynein/dynactin motor protein complex transports cargo from the tip of the axon towards the neuronal cell body (retrograde direction). There have been several neurodegeneration disorders linked to mutations in dynein and dynactin genes (Levy and Holzbaur, 2006). This suggests that mammalian neurons are particularly sensitive to the dynein/dynactin mutations. A potential reason why neurons could be especially sensitive to the motor complex mutations will be discussed later.

1.3 Dynein structure and function

A dynein molecule (Fig.3) is about 1.2 mega Dalton in mass and is comprised of various subunits. The dynein subunits arranged in a motor complex are - 2 dynein heavy chains (DHCs), 2 dynein intermediate chains (DICs), 4 dynein light intermediate chains (DLICs) and 3 pairs of dynein light chains (DLCs). The tail region of DHCs interacts with the DLICs and together they interact with various other subunits (King et al., 2002). The

DICs have many interacting protein partners like dynactin, Bicaudal D (Bic D) (Hoogenraad et al., 2001), Lissencephaly (LIS 1) (Smith et al., 2000), Nuclear distribution protein E (NudE) (McKenney et al., 2010). Together these additional binding partners help dynein to be more adaptable to carry a variety of cargoes inside the cell. Overall, dynein carries out various important cellular processes like cargo trafficking (Traer et al., 2007), nuclear migration (Levy and Holzbaur, 2008), chromosome segregation during mitosis (Dujardin et al., 1998), cell division (Pfarr et al., 1990) and organelle positioning (Burkhardt et al., 1997).

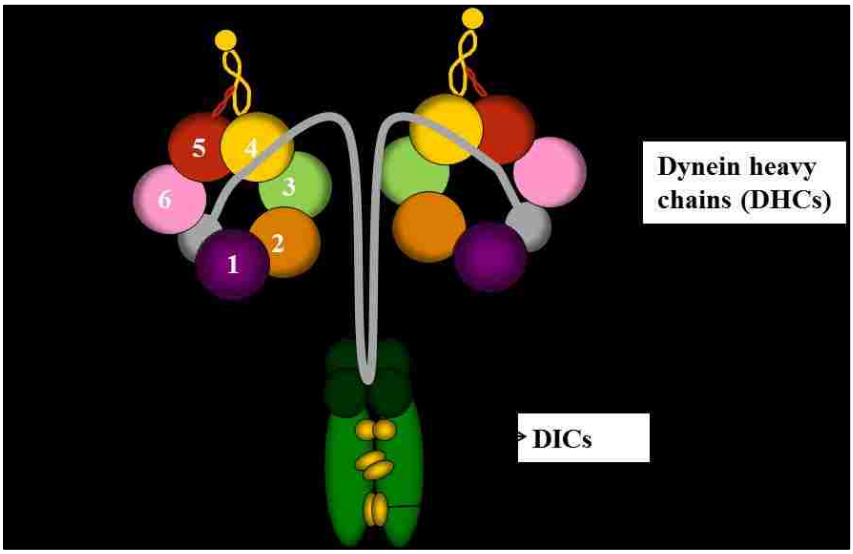

Figure 3: Dynein molecule structure

A dynein molecule comprises of 2 dynein heavy chains, 2 intermediate chains (shown in light green), 4 light intermediate chains (shown in dark green) and 3 pairs of light chains (shown in yellow).

The DHC subunits of dynein have the main role in the motor activity of the dynein. The DHCs participate in the transport process by hydrolyzing the ATP and generating force to take steps on the microtubule. Hence, the next subsection will explain the structure and the motor function of the DHCs, to better understand its importance in intracellular transport.

1.3.1 Dynein heavy chain

The DHC is ~4500 amino acids long and is a member of the AAA+ domain protein family. The DHC can be divided into two regions – an N-terminus tail domain and a globular head domain (Fig.4 A). The N-terminal ends of two DHCs coil together and form a homodimer tail at the base of the dynein molecule. The tail domain regulates dynein and interacts with other dynein subunits and cargoes.

The globular head domain has motor activity and contains 6 repeating units of AAA+ (ATPase Associated with various cellular Activities) ATPase sites arranged in a ring (AAA1-AAA6) (Burgess et al., 2004; Sakato and King, 2004). The AAA1 domain has a p-loop motif that binds and hydrolyzes ATP (Gibbons et al., 1991; Gibbons et al., 1987; Koonce et al., 1992). Other domains, AAA2-AAA4 also have p-loop motifs and can bind ATP but appear incapable or less capable of hydrolyzing ATP. These secondary sites may serve as dynein function regulators (Mocz and Gibbons, 1996).

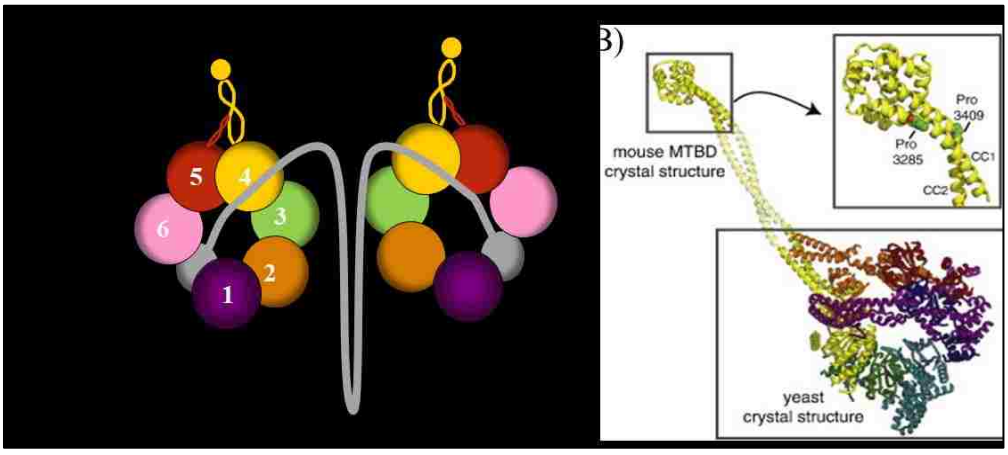

Figure 4: Dynein Heavy Chains (DHCs) structure

Left: The DHC has 2 regions- N terminus tail domain and a globular motor head. Right: The DHC crystal structure showing various globular motor domains with the microtubule binding domain (MTBD) crystal structure arising from it. (Adapted from Vale et al. 2012; *Biochimica et Biophysica Acta*)

The AAA5-AAA6 domains lack ATP binding and ATPase enzymatic activity (Neuwald et al., 1999), but act as structural supports to complete the ring structure of the dynein molecule. Dynein's microtubule binding stalk is located between the AAA4 and AAA5 domains(Koonce, 1997).

Recently, DHC crystal structures have been published (Carter et al., 2011; Kon et al., 2011) and they show various structural features of the dynein molecule (Fig.4 B). These crystal structures give a better understanding of how the 6 AAA+ ATPase domains in the DHC globular head interact with each other. The DHC crystal structures also shows specific position of other dynein domains such as the linker, strut, and microtubule binding stalk and how they can help in nucleotide sensing and the motor function (Fig.4B).

1.4 Dynactin structure and function

Structurally, dynactin is ~ 1 mega Dalton molecule (Fig.5) and contains 11 different subunits (Schroer, 2004). These dynactin subunits interact with dynein, microtubules and cargos. The largest dynactin subunit, p150, is ~1300 amino acid long and forms a dimer via a coiled coil region (CC-1). The CC-1 region interacts with the dynein intermediate chains (King et al., 2003) and overexpression of this domain has been used to uncouple dynein/dynactin function (Kwinter et al., 2009; Quintyne et al., 1999). The overexpressed CC-1 domains bind strongly to dynein motors and outcompete the binding of dynactin to the dynein. Thus, in a CC-1 overexpressing cell, the vast majority of dynein cannot bind dynactin but instead are bound to CC-1.

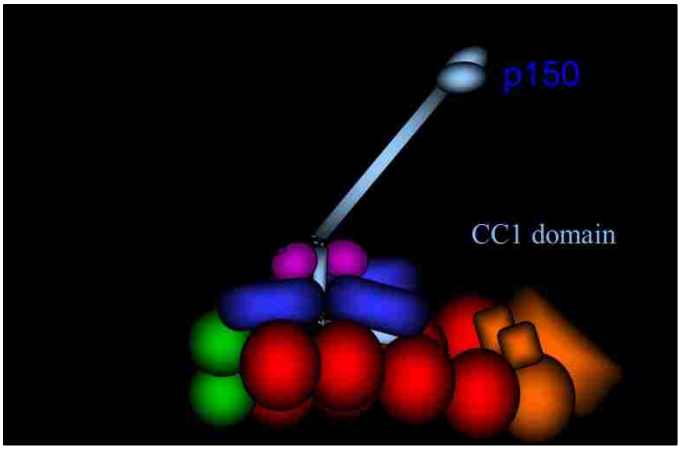

Figure 5: Dynactin molecule structure

The microtubule binding domain (MTBD) of dynactin contains the p150 subunit. Dynactin binds to the dynein through CC-1 domain. Other dynactin subunits (such as p25, p27, p50/dynamitin, p62, Arp1and Arp 11) interact and bind to the cargo.

The p150 subunit has two microtubule binding domains (MTBD) at the N terminus. The first MTBD contains a conserved glycine rich CAP-Gly region (Fig.6, shown in green) and the second MTBD part contains a highly basic region (Fig.6, shown in blue). The CAP-Gly MTBD is needed for cargo attachment onto the microtubule and initiation of dynein/dynactin transport process (Moughamian and Holzbaur, 2012). The basic MTBD of p150 has a role in the processivity enhancement of the dynein/dynactin motor complex (Culver-Hanlon et al., 2006; Kincaid and King, 2006).

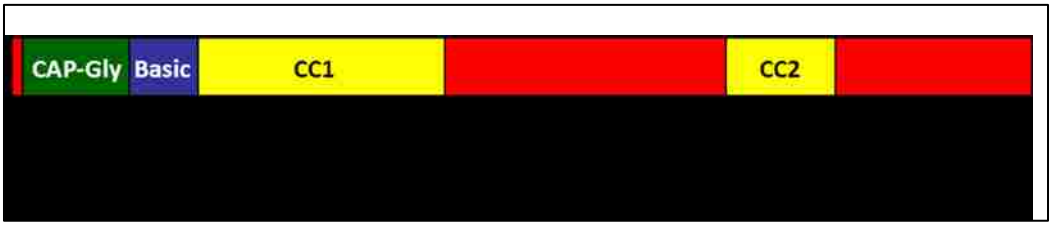

Figure 6: The p150 subunit of dynactin

Dynactin p150 contains 2 microtubule binding domain (MTBD): a glycine rich CAP-Gly region (shown in green) and a highly basic region (shown in blue). The MTBDs are followed by the two coiled coil regions CC-1 and CC-2 (shown in yellow) and some regions of unknown function (red). The CC-1 domain interacts with the dynein molecule.

The cargo binding domain of dynactin (Fig. 5) contains many subunits including p25, p27, p50/dynamitin, p62, Arp1 and Arp 11 that can bind to variety of different cellular cargoes (Schroer, 2004). For example, some dynactin subunits such as the filamentous actin related protein Arp1 interacts with the Golgi complex via spectrin linkages (Holleran et al., 2001) and the p50/dynamitin subunit interacts with the mitotic checkpoint proteins such as ZW10 (Starr et al., 1998).

1.5 Role of the dynein-dynactin motor protein complex in neurodegeneration

The dynein/dynactin motor complex has a role in the highly processive transport system required by neurons to carry essential molecules over long range distances. Consequently, mutations in the dynein/dynactin motor complex could potentially have a pronounced effect on neurons because of their long axonal morphology. For example, with normal velocity of 1μm/sec, the dynein/dynactin motor complex takes about 10 seconds to transport cargo across a typical 10μm animal cell and takes more than 10 days to transport cargo in a 1 meter long neuron. In case there is a mutation in the dynein/dynactin complex that decreases its dynein velocity from 1μm/sec to 0.5μm/sec. Now, the mutant dynein/dynactin complex would take 20 seconds to deliver the same cargo across a 10μm animal cell, which may not cause an adverse effect. However, the same mutant dynein would take more than 20 days instead of 10 days to transport a cargo in a long neuron. This delay might cause a defect that leads to severe degradation of neuronal health. Hence, it seems apparent that there is a need for robust dynein/dynactin motor complex transport system inside neurons at all times to avoid defects in intracellular transport that may lead to neurodegeneration. In support of this concept,

there have been many neurodegeneration linked mutations identified in the dynein/dynactin motor protein complex as described in the following sections.

1.5.1 Neurodegeneration linked mutations in dynein

There are several human neurological disorders linked to mutations in the DHCs. A mutation was found in the DHC tail's homodimerization domain where the histidine at 306 position gets replaced by an arginine residue (H306R). This H306R mutation in the DHCs was identified in the human patients suffering from the Charcot Marie Tooth (CMT) type 2O disease (Weedon et al., 2011). CMT type 2O is a motor neuron disease that causes impairment in the motor functions, gait abnormalities and arched feet (pes caveus) deformities in patients.

Other neurodegeneration linked mutations - K671E, Y907C and I584L, in the tail region of the human DHC have been identified (Baloh et al., 2012). These mutations were identified in the human patients suffering from the Spinal Muscular Atrophy with Lower Extremity Predominance (SMA-LED). Some manifestations of the SMA-LED disorder in the patients included distal neuropathy, significant motor delay in infancy, muscular atrophy and proximal predominant leg weakness, waddling gait, awkward running and mild cognitive delay.

In some patients other DHC mutations were identified – H3822P (Vissers et al., 2010) and E1518K (Willemsen et al., 2012). These mutations caused neuronal migration defects, developmental delays, cortical malfunctions, severe speech impairment, intellectual inability and mental retardation, waddling gait and reduced tendon reflexes.

Three other DHC mutations have been identified in mice, which are a common model system to study neurodegeneration (Chen et al., 2007; Duchen, 1974; Hafezparast et al., 2003). These mutant mice are Cramping (*Cra* 1), Legs at odd angles (*Loa*) and Sprawling (*swl*) and they developed neurodegenerative defects. These neurodegenerative mutant mice displayed flaws in their posture and motor coordination. When these mice were subjected to the tail suspension test, they displayed abnormal clasping and clenching of their hind limbs and toes (Banks and Fisher, 2008). With time these heterozygous mutant mice developed late onset of motor neuron disorders. Further characterizations of *Cra1* and *Loa* mice neurons revealed impaired motility associated with reduced dynein processivity (Hafezparast et al., 2003; Ori-McKenney et al., 2010).

To conclude, mutations in the DHC region have been reported to cause neurodegenerative phenotypes in humans and in mice. A very interesting point is that all of the known mutations in the DHC have been linked to neurodegenerative disorders. There are no other DHC mutations that cause other types of diseases, suggesting that neurons are the most sensitive to the defects in dynein function. Another point to note is that no neurodegeneration linked mutations have been reported in other components of dynein (DICs, DLCs and DLICs).

1.5.2 Neurodegeneration linked mutations in dynactin

There are several disease linked mutations in the p150 subunit of dynactin (Fig.7) that are linked to human neurodegenerative diseases. For example, the G59S mutation in the CAP-Gly region of the p150 subunit of dynactin has been linked to distal Spinal Bulbar Muscular Atrophy (dSBMA) (Chevalier-Larsen et al., 2008). The patients

suffering from dSBMA have an onset of progressive motor neuron disorder, paralysis in the vocal cords and/or weaknesses in face, hand and lower extremities (Puls et al., 2003). Mutant mouse models having G59S mutations showed motility defects and developed disease conditions related to motor neuron disorders (Lai et al., 2007). Another set of mutations (G71E, G71A, G71R, T72P and Q74P) in the same CAP-Gly region leads to Perry syndrome (Farrer et al., 2009). Perry syndrome characteristics involve Parkinsonism, hypoventilation, weight loss and depression in humans in their late 40s or 50s. Other mutations (M571T, R785W, R1101K and T1249I) near the CC-1 and CC-2 domain of dynactin have been linked to Amyotrophic lateral sclerosis (ALS) (LaMonte et al., 2002), but no further work has been reported on these mutations.

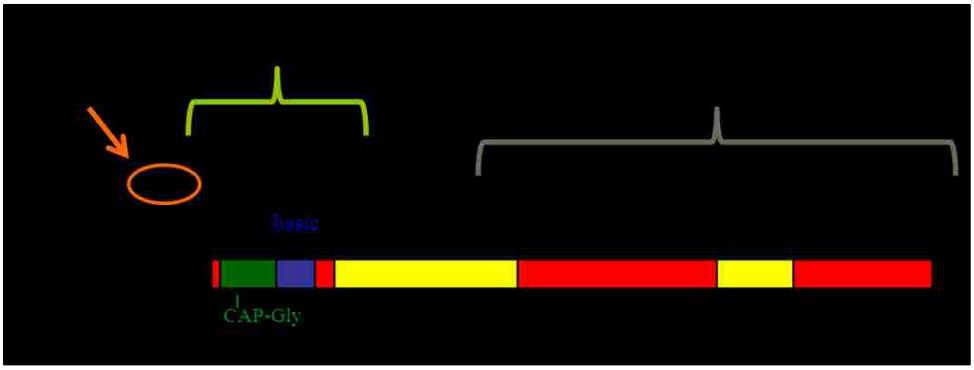

Figure 7: Neurodegenerative linked mutations in dynactin

Localization of neurodegenerative disorders (dSBMA, Perry syndrome and ALS) linked mutations in dynactin.

1.6 Hypothesis: Dynein/dynactin motor protein complex and Neurodegeneration

It is very intriguing that all of the known mutations in dynein and dynactin cause neurodegenerative disorders and no other types of diseases. As discussed previously, the morphology of long axons might make neurons more sensitive than other cell types to potential transport defects caused by mutations in the dynein/dynactin motor protein

complex. In contrast, severe dynein mutations (DHCΔ) result in the death of complex organisms (Harada et al., 1998). However, some mutations in the dynein/dynactin motor complex can moderately alter the intracellular transport in neurons and instead cause neurodegenerative phenotypes.

Based on the abovementioned line of conjecture, the King lab has developed a hypothesis*: Neurodegenerative phenotypes of mutations in the dynein/dynactin motor protein complex are due to subtle, and not severe, defects in intracellular transport.*

To test this hypothesis, our aim is to study the effects of dynein/dynactin motor complex mutations on the long neuronal transport. But due to the inherent difficulties of working with neuronal cultures, my own approach was to use simpler cell systems to set a ground work to initially test the effects of dynein and dynactin disruptions on intracellular transport. In the approach detailed in Chapter 2, the effects of several spontaneous DHC mutations on transport were characterized in the fungi *Neurospora crassa*. In another set of experiments detailed in Chapter 3, the dynein/dynactin complex was disrupted in the mammalian CAD cell line and consequent effects on mitochondrial motility were studied. In support of our hypothesis, in each experiment I was able to determine that a moderate loss of dynein/dynactin function correlated with subtle transport defects whereas severe loss of dynein/dynactin function resulted in more severe phenotypes that would likely cause cells to die.

CHAPTER 2: *N. crassa* MOTILITY ANALYSES

2.1 Introduction: *N.crassa* as a model system to study dynein function

In most eukaryotes, dynein is an essential protein for cell survival and is needed to carry out many necessary functions during embryonic development. Total loss/deletion of dynein causes early embryonic lethality in homozygous DHCΔ animals (Hafezparast et al., 2003; Harada et al., 1998). Hence, there is a challenge to carry out dynein alterations and mutational analyses in many eukaryotic systems. However, dynein is not essential for *N. crassa* survival and the gene can be mutated or altered in a variety of genetic ways. Moreover, the *N. crassa* has a haploid genome, which has the advantages that 1) all effects/phenotype of the mutation will be observed since there are no recessive/dominant allele expression, 2) all proteins present have same genetic basis so all dynein would be equal and 3) the uniformity of genetic alteration can be established in the pool of all the dynein motors.

Hence for one aspect of my Thesis project, I studied and characterized the motility parameters of various spontaneous DHC mutations developed in *N. crassa*. I characterized the vesicular transport in Wildtype (WT) and DHC mutant strains using live cell imaging followed by kymograph analyses.

2.2 Background work on *N. crassa*

2.2.1 The *ropy* mutants

A collaboration between the King and Plamann Lab (University of Missouri, Kansas City) made use of a genetic trick with the colonial temperature sensitive (*cot-1*^{ts}) mutant strain to study dynein function in *N. crassa* (Plamann et al., 1994). The *cot-1*^{ts}

mutant strain of *N. crassa* grows like the wildtype strain at the permissive temperature (28°C) with normal radial colony morphology. When the temperature is raised to 37°C, the *cot-1*^{ts} mutant strain shows a constrained growth (Fig 8). At a low frequency some *N. crassa* colonies undergo spontaneous mutations in genes that suppress the temperature sensitivity of the *cot-1*^{ts} strain at 37°C. These suppressed colonies are able to grow at the restrictive temperatures (37ºC). When these suppressed colonies are isolated and grown back at the 28°C permissive temperature, they grow as *ropy* mutant colonies having highly branched hyphae.

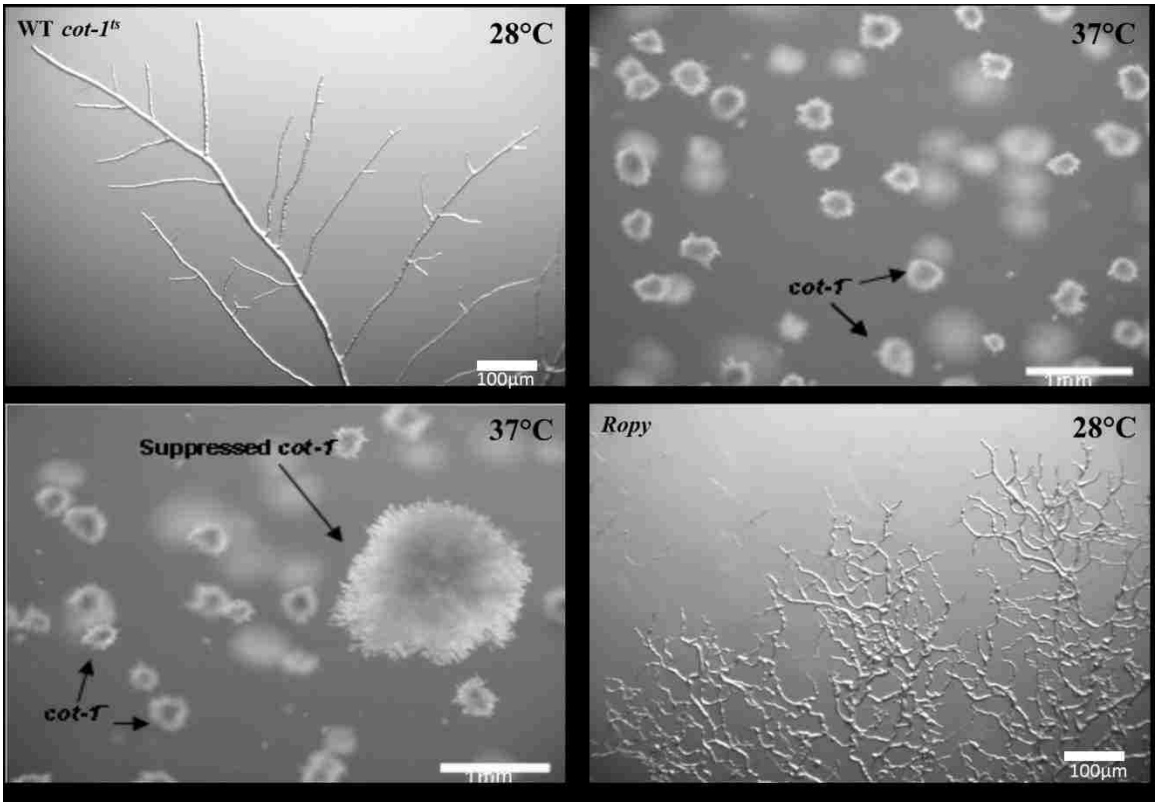

Figure 8: The *ropy* mutant colony morphology

The *cot-1*^{ts} is a temperature sensitive strain of *N. crassa* (top left panel) and has a suppressed growth at the restrictive temperature of 37°C (top right panel). Revertant colonies pick up mutations to suppress the *cot-1*^{ts} mutation and grow at 37°C (bottom left panel). When grown back at 28°C, these *cot-1*^{ts} suppressant colonies have highly branched hyphae with *ropy* phenotype (bottom right panel). (Adapted from Sivagurunathan et al., 2012; *Genetics*)

2.2.2 Isolation of *N. crassa* DHC class mutants

For a collaborative project between the King Lab and the Plamann Lab, several hundred of these *cot-1*^{ts} suppressant *ropy* colonies were isolated and characterized (Sivagurunathan et al., 2012b). Several sequential identification steps (Fig. 9) were applied on the isolated *ropy* mutant colonies.

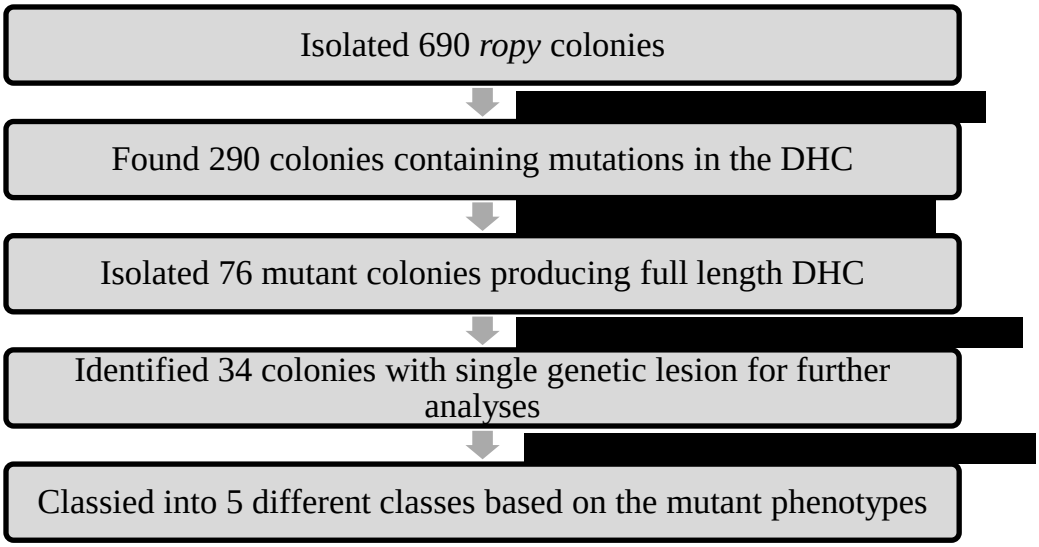

Figure 9: Isolation of *N. crassa* DHC class mutants

The flowchart shows the steps followed to isolate, identify and classify various *N. crassa ropy* mutant strains. The text next to the arrows indicates the procedural action followed to achieve the next mentioned step.

Out of 690 mutant colonies, 290 *ropy* mutant colonies were isolated that had mutations only in the DHC gene. The remaining 400 mutant colonies had defects in other components of dynein and dynactin and were not analyzed further. Western blot was performed on the 290 DHC mutant colonies to identify which of those colonies produced full length DHC. 76 mutant colonies were isolated that produced full length DHC and those mutations were sent for DNA sequencing. From DNA sequencing it was identified that 44 colonies had a frameshift or nonsense mutation in the DHC and were discarded,

except for 2 frameshift mutants that produced slightly shortened DHC. These 2 mutants were considered for analysis along with 32 other mutant strains that had only single point mutations in the DHC region.

Next, these 34 *ropy* mutant strains were crossed with a *N. crassa* strain having mCherry tagged DIC and GFP labeled tubulin. This step was performed to identify the localization of dynein and the microtubules in *ropy* mutants. Based on the immunofluorescence microscopy and biochemical assays, these 34 *ropy* mutants were then classified into 5 different classes of DHC mutant phenotypes (Fig.10) (Sivagurunathan et al., 2012b).

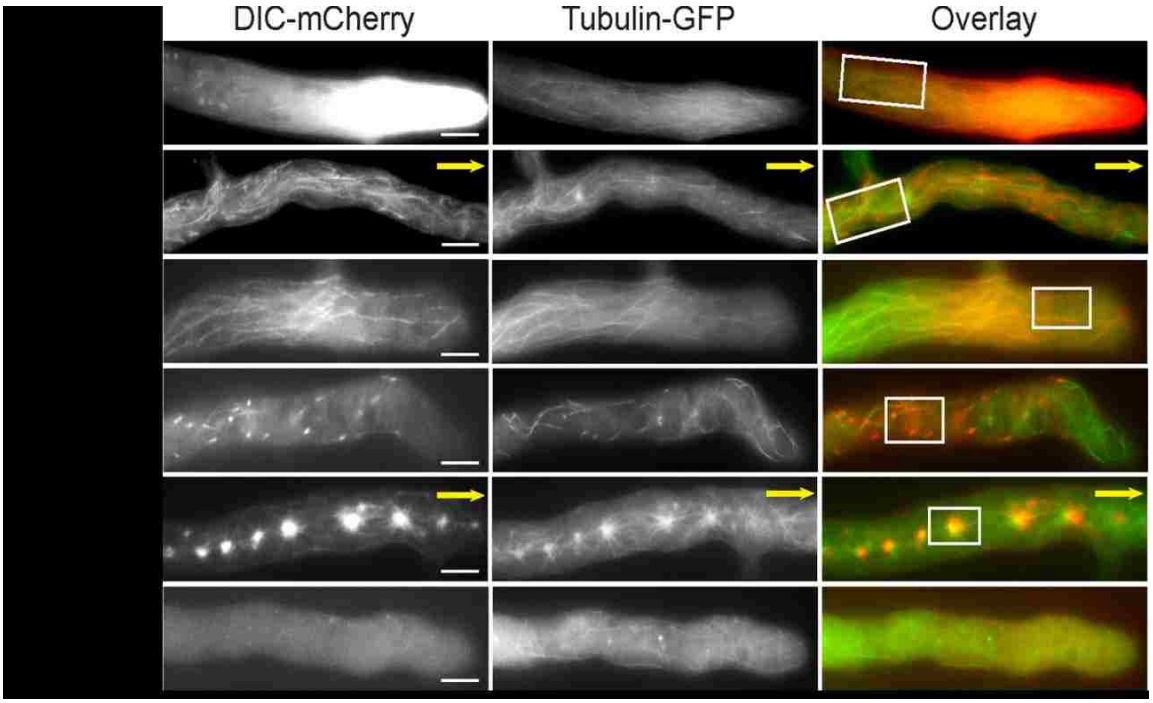

Figure 10: Comparison of DHC class mutant phenotypes

The images show different phenotypes of DHC class mutants as compared to the Wildtype (WT) phenotype. The first column shows the dynein localization (red channel) and the second column shows the microtubule localization (green channel) in hyphae. The third column shows a merged image of the red and the green channel. Scale bar = 10µm. (Adapted from Sivagurunathan et al., 2012; *Genetics*)

In the wildtype (WT) *N. crassa* hyphae, the dynein was localized as a bright pool in the hyphal tip (Fig.10) and was dimmer at other locations in the hyphae. However for the 5 different DHC mutant classes, the dynein localization at the bright hyphal tip was abolished. In DHC mutant strains, the dynein got localized to the other locations such as away (distal) from the hyphal tip (Class 1), near (apical) the tip (Class 2), on the MT ends as comets (Class 3), clustered in aggregates (Class 4) and diffused along the hyphae (Class 5). The microtubules in the DHC class mutant strain were also disorganized in comparison to the microtubules in the WT hyphae. Also, the hyphal tips of the DHC class mutants grew at a slower rate as compared to the WT strain.

It was found that these 34 DHC mutations spanned all through the 6 AAA+ ATPase domains and the tail region (Fig.11A). Also, these mutations could be mapped on a DHC crystal structure (Fig.11B) to correlate between the position of these mutations in the DHC and the resultant mutant phenotype. Interesting things can be learned from the mutations mapping on crystal structure. For example, it seems that the Class 5 mutations highlighted in orange are all over the DHC polypeptide (Fig. 11A), but from the crystal structure it can be seen that Class 5 mutations are localized close to each other (Fig. 11B). Similarly, Class 1 mutations (highlighted in blue) that are localized in different domains on the DHC polypeptide can be seen localized near each other on the DHC crystal structure. Hence, it is useful to have the DHC polypeptide mutations be mapped onto a crystal structure as it gives a better visualization of how the mutations localize on a three dimensional globular DHC structure may share common mechanisms of action.

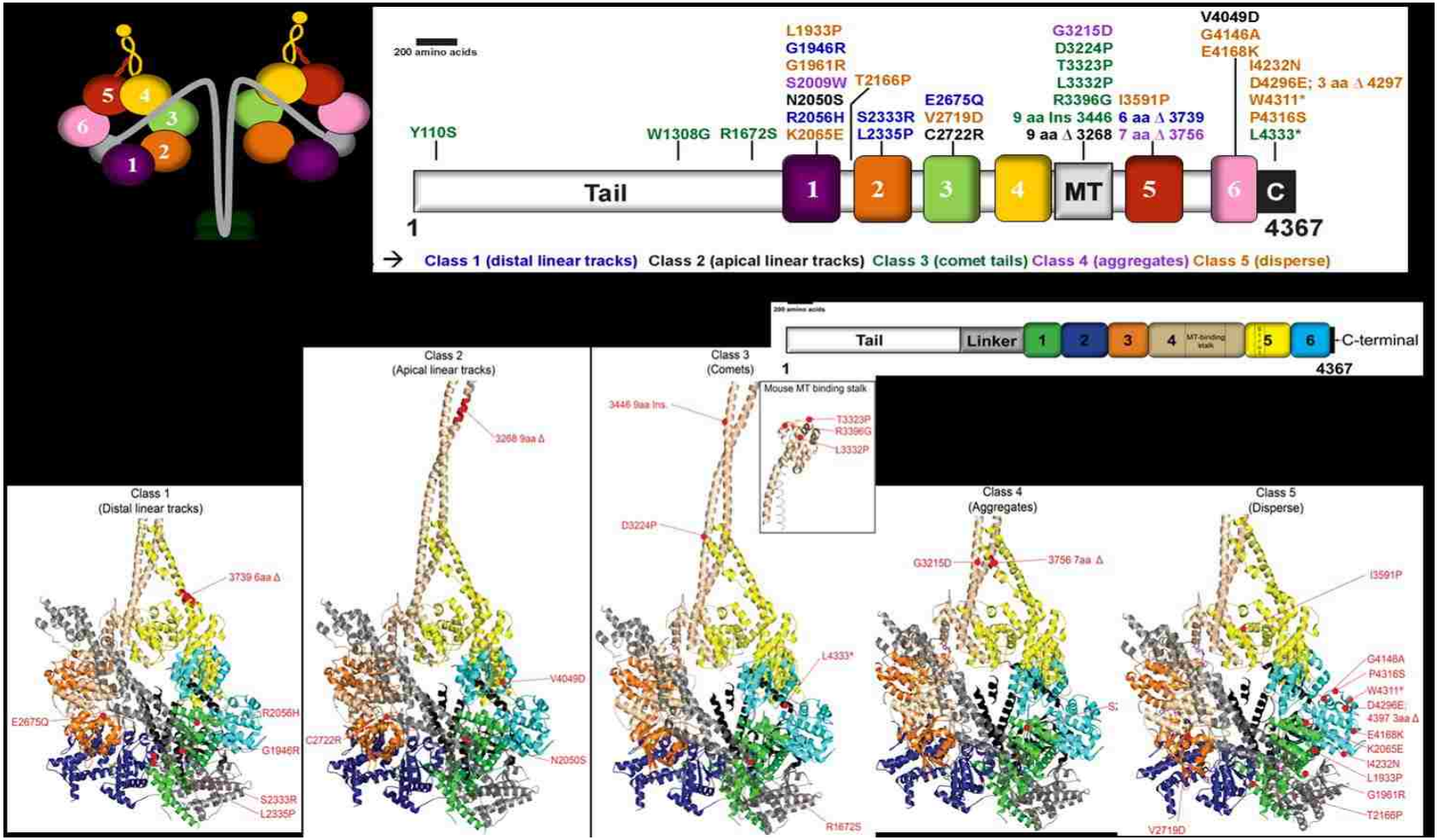

Figure 11: Localization of DHC class mutations

The DHC class mutations were mapped on the DHC polypeptide (A) and on the DHC crystal structure (B). The 34 DHC mutations span across all ATPase domains as well as the tail region of the DHC polypeptide. (Adapted from Sivagurunathan et al., 2012; *Genetics*)

2.2.3 Generation of *N. crassa Loa* mutants

The collaborating labs were also interested to see what phenotypes *N. crassa* would develop with neurodegenerative mouse mutant dynein alleles. Hence, they decided to make a *N. crassa Loa* mutant strain.

A *Loa* mutant mouse with a missense mutation F580Y in the DHC tail region develops neurodegeneration. This F580Y mutant heterozygous mouse had abnormal posture, defects in neuronal migration, muscle weakness and late onset of motor neuron disorder (Banks and Fisher, 2008). During a tail suspension test (Fig.12), the mutant mouse clasped its hind limbs together and displayed an abnormal phenotype of *legs at odd angle* and acquired its name as *Loa* (Legs at odd angle) mouse.

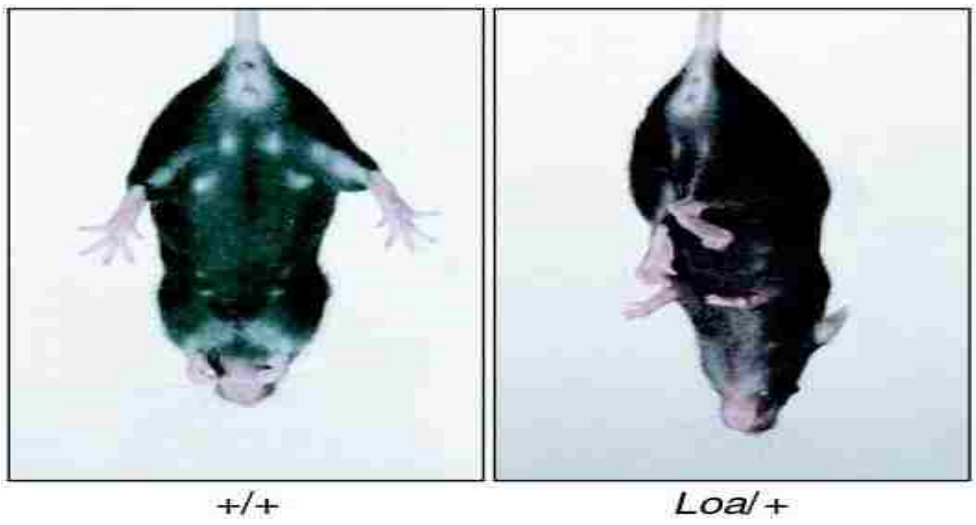

Figure 12: Tail suspension test

Left: A wildtype mouse displaying normal splayed hind limb phenotype during the tail suspension test. Right: A mutant *Loa* heterozygous mouse displaying abnormal "*Legs at odd angle*" phenotype during the tail suspension test. (Adapted from Fisher et.al 2008, *Genome Biology*)

The neurons extracted from the heterozygous *Loa*/+ mouse showed a slight defect in the retrograde axonal transport of lysosomes (Ori-McKenney et al., 2010). The

homozygous *Loa/Loa* mouse was embryonic lethal and the neurons extracted from it showed a significant defect in the retrograde axonal transport (Hafezparast et al., 2003).

The same *Loa* mutation was studied and characterized in *N. crassa* (Sivagurunathan et al., 2012a). Due to the structural conservation of DHC (Fig.13) between *N. crassa* and the higher eukaryotes, it was possible to generate the corresponding *Loa* mutation (F607Y) in the *N. crassa* DHC tail region.

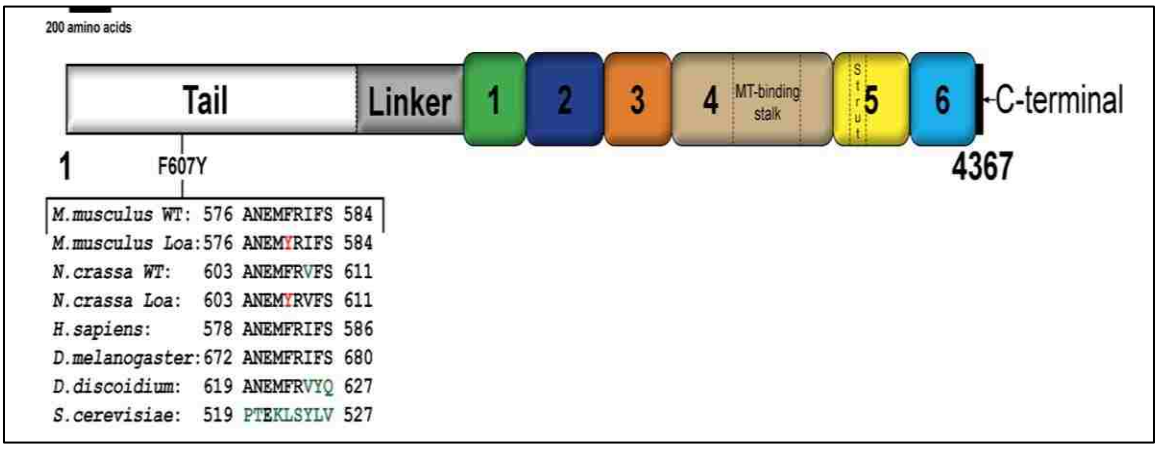

Figure 13: *Loa* tail mutation in *N. crassa* DHC

Structural conservation of DHC exists between *N. crassa* and the higher eukaryotes. This makes it possible to generate mouse neurodegenerative *Loa* mutation in *N. crassa*. The *Loa* mutation is a F607Y missense mutation in the DHC tail region. . (Adapted from Sivagurunathan et al., 2012; *Cytoskeleton*)

The hyphal morphology of mutant *Loa N. crassa* (Fig.14) was intermediate between that of WT and *ropy* DHC class mutants. Also, the dynein pool at the hyphal tip of the *Loa* mutant strain was reduced as compared to the WT hyphae, but it was not completely abolished like what was observed for the 5 DHC *ropy* class mutants (Fig.10). Now, the next question was if the DHC class mutations and the *Loa* mutation cause any defects in the vesicular transport of *N. crassa.*

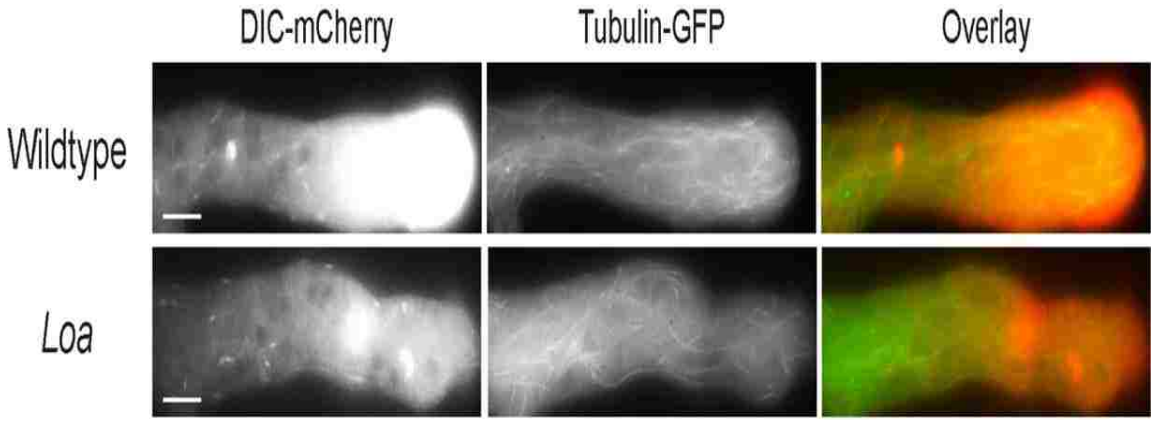

Figure 14: Localization of dynein in the mutant *Loa N. crassa* strain

First column shows the dynein localization (red channel) and the second column shows the microtubule localization (green channel) in the *N. crassa* hyphae. The third column is a merged image of the red and green channel. Compared to the wildtype strain, the dynein localization is reduced at the hyphal tip in the *Loa* mutant. Scale bar = 10µm. (Adapted from Sivagurunathan et al., 2012; *Cytoskeleton*)

2.3 Results and discussion

2.3.1 *N. crassa* DHC class mutants results

Mutations in the DHC affected dynein localization in *N. crassa* hyphae. The transport of FM 4-64 labeled vesicles in the growing hyphal tip of WT and DHC mutants were recorded using live cell imaging and the motility analysis was performed using kymographs.

2.3.1.1 Kymograph and motility analyses

Kymographs were plotted and analyzed to study the motility patterns of the FM 4-64 labeled vesicles in *N. crassa* hyphae.

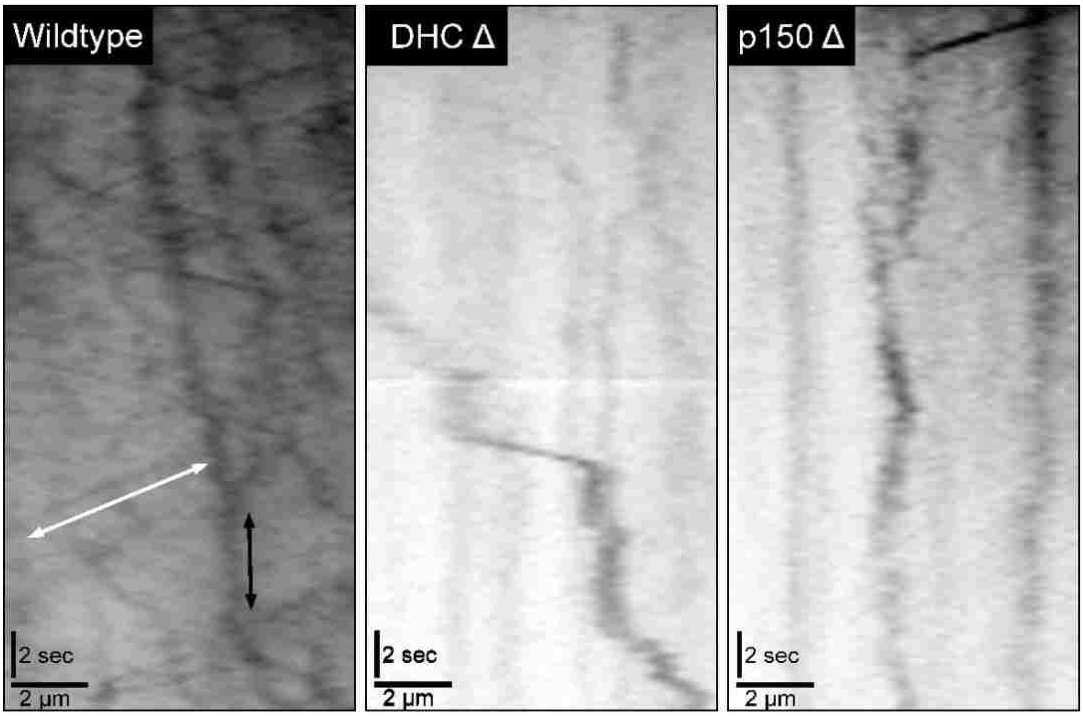

Figure 15: Kymographs of the FM® 4-64 labeled vesicles in *N. crassa* hyphae

Kymographs (i.e. distance vs. time graphs) for various *N. crassa* controls – Wildtype (WT), DHCΔ and p150Δ. On a kymograph, the diagonal line (white arrow) represents a moving vesicle and the vertical line (black arrow) represents a stationary vesicle. Less number of diagonal lines is present in the DHCΔ and p150Δ mutant strains indicating lesser motility events than the WT. (Adapted from Sivagurunathan et al., 2012; *Genetics*)

In WT kymograph (Fig.15), there were numerous diagonal lines representing high amount of vesicular motility inside the WT hyphae. But for the control mutant strains (DHCΔ, p150Δ and *Nkin*) and the DHC class mutant strains (Classes 1-5), less number of diagonal lines were present on the respective kymographs (Fig. 15 & 16). This signifies that there was a decrease in the number of motility events inside the *N. crassa* mutant hyphae.

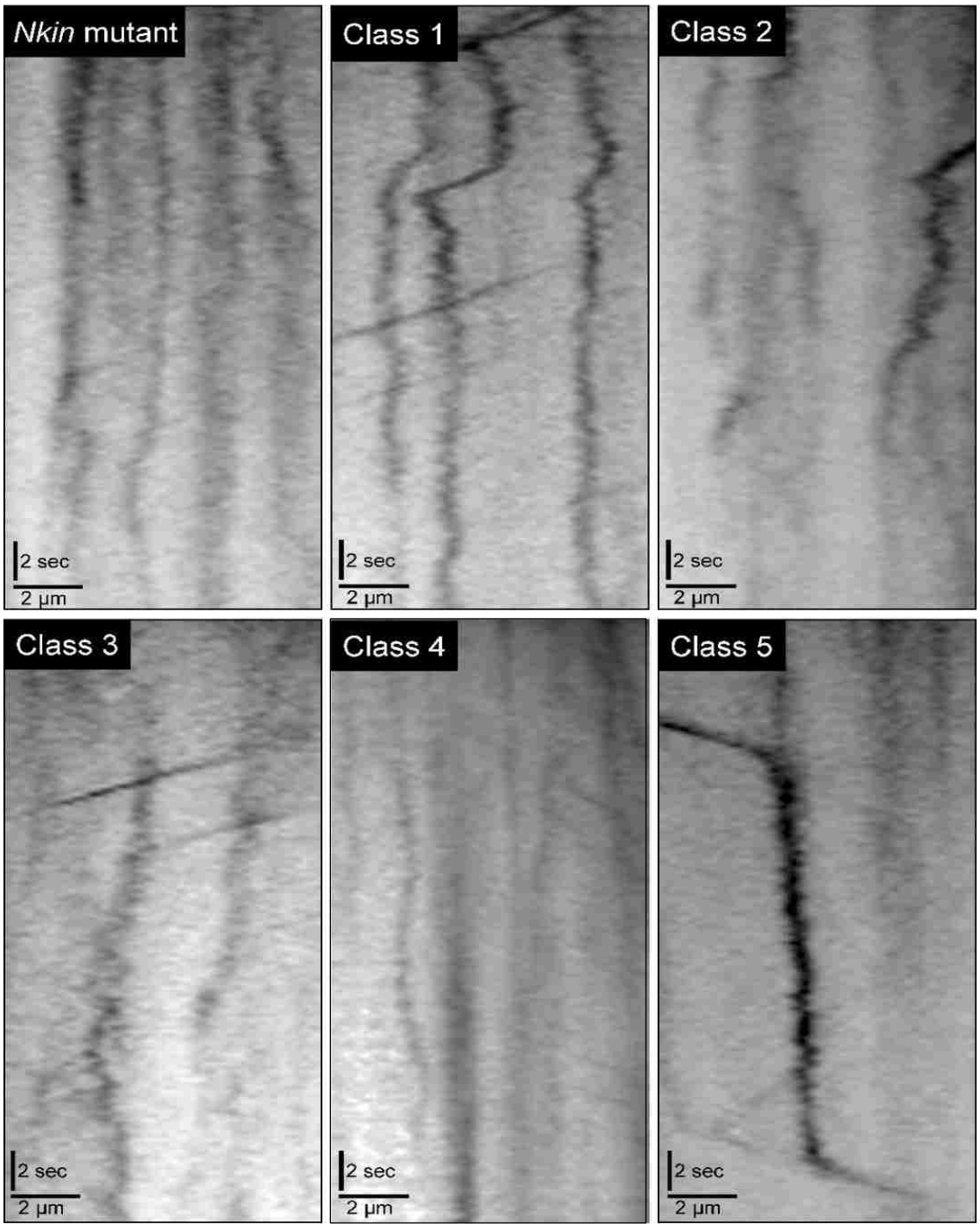

Figure 16: Kymographs of *N. crassa* mutant strains

Kymographs (i.e. distance vs. time graphs) for various *N. crassa* mutant strains show less number of diagonal lines indicating lesser motility events than the WT. (Adapted from Sivagurunathan et al., 2012; *Genetics*)

Data on various motility parameters such as run lengths, velocities and the number of movements were generated for FM 4-64 labeled vesicles based on the *N. crassa* (WT and mutant) kymographs.

Compared to the *N. crassa* WT strain, the DHC class mutant strains showed a decrease in various motility parameters (Table 1). Overall, there was about 50-80% reduction in the motility index for the DHC mutant strains as compared to the WT. Also, I observed a decrease in the mean movements of vesicles happening over a micron length of mutant hyphae strains. Correspondingly, less number of vesicular movements (*N*) was recorded for the mutant strains than for the WT.

For all the DHC class mutants and controls (Table 1), I determined that there was a significant decrease in the mean velocity of the vesicular movements. In addition to that, a significant decrease was also seen in the mean distances travelled by the vesicles in most of the mutant strains, except for Class 1 and Class 5. Hence, it can be concluded that most of the DHC mutations affected the overall intracellular transport, as seen by the decrease in the mean velocity and distance. To get an assessment of overall motility measures, an index was generated by combining all the motility parameters. That is, the motility index was calculated by adding all the distances multiplied with respective velocities for all the motility events and that value was divided by the total hyphal length analyzed.

$$\text{Motility index} = \frac{\sum (\text{Distance} \times \text{Velocity})}{\text{hyphal length analyzed}}$$

Table 1: Comparison of motility parameters for the *N.crassa* WT and mutant strains

	Wildtype	DHC Δ	p150 Δ	Nkin mut.	Class 1	Class 2	Class 3	Class 4	Class 5
Motility index	21.5	5.8	8.3	4.1	10.4	4.9	9.4	7.4	6.2
Overall movements									
Mean movements/ µm hyphal length	2.9	1.2	1.8	0.8	1.5	1.2	2.4	1.7	1.1
N	557	185	286	162	199	110	247	200	170
Mean velocity (µm/sec ± S.D.)	1.64 ± 0.59	1.46 ± 0.62*	1.34 ± 0.49*	1.35 ± 0.52*	1.51 ± 0.59*	1.24 ± 0.41*	1.33 ± 0.45*	1.33 ± 0.41*	1.31 ± 0.48*
Mean distance (µm ± S.D.)	4.26 ± 0.54	3.03 ± 1.71*	3.19 ± 1.44*	3.49 ± 2.07*	4.48 ± 2.59	3.21 ± 1.64*	2.85 ± 1.15*	3.17 ± 1.33*	3.96 ± 2.33

Various motility parameters are listed out for the Wildtype (WT), controls and the DHC class mutant strains. The table shows the overall motility events of the vesicles travelling in all the directions inside the hyphae. The '*' indicates statistically significant difference from the WT value as determined by the Student's T-test ($P < 0.05$). . (Adapted from Sivagurunathan et al., 2012; *Genetics*)

Table 2: Vesicle accumulation in *N. crassa* hyphae

	Wildtype	DHC Δ	p150 Δ	Nkin mut.	Class 1	Class 2	Class 3	Class 4	Class 5
Vesicle accumulation									
Hyphal tip vesicle accumulation	60.0 %	92.3 %	27.3 %	100 %	72.7 %	86.7 %	90.0 %	78.6 %	100 %
Hyphal body vesicle accumulation	13.3 %	7.7 %	90.9 %	0 %	9.1 %	6.7 %	20.0 %	21.4 %	0 %

The percentage (%) represents the number of movies that display the mentioned vesicle accumulation phenotype out of the total number of movies. The p150Δ strain has the altered ratio of vesicle accumulation and is highlighted in red to indicate the difference with respect to the WT. (Adapted from Sivagurunathan et al., 2012; *Genetics*)

Table 3: Comparison of motility parameters for the inward and the outward directed vesicular movements

	Wildtype	DHC Δ	p150 Δ	Nkin mut.	Class 1	Class 2	Class 3	Class 4	Class 5
Inward movements									
Percent of total movements	48.7 %	47.1 %	48.9 %	48.8 %	41.7 %	52.7 %	53.8 %	41.5 %	47.1 %
Mean velocity (µm/sec ± S.D.)	1.60 ± 0.55	1.36 ± 0.53*	1.27 ± 0.51*	1.36 ± 0.53*	1.43 ± 0.54*	1.23 ± 0.45*	1.29 ± 0.48*	1.24 ± 0.40*	1.28 ± 0.53*
Mean distance (µm ± S.D.)	4.16 ± 2.47	2.70 ± 1.27*	2.78 ± 1.12*	3.23 ± 1.88*	3.90 ± 2.62	2.86 ± 1.38*	2.69 ± 1.02*	2.66 ± 0.96*	3.77 ± 2.40
Outward movements									
Percent of total movements	51.3 %	52.9 %	51.1 %	51.2 %	58.3 %	47.3 %	46.2 %	58.5 %	52.9 %
Mean velocity (µm/sec ± S.D.)	1.67 ± 0.61	1.55 ± 0.69	1.41 ± 0.47*	1.35 ± 0.51*	1.56 ± 0.62	1.24 ± 0.36*	1.38 ± 0.42*	1.40 ± 0.41*	1.35 ± 0.44*
Mean distance (µm ± S.D.)	4.36 ± 2.60	3.32 ± 1.98*	3.59 ± 1.59*	3.75 ± 2.22*	4.89 ± 2.49	3.57 ± 1.83*	3.05 ± 1.27*	3.53 ± 1.45*	4.13 ± 2.26
*** = statistically significant difference from wild-type value as determined by students t-test (P < 0.05).**									

Various motility parameters are listed out for the Wildtype (WT), controls and the DHC class mutant strains. The table shows the overall motility events of the vesicles travelling in the inwards and the outward directions inside the hyphae. The '*' indicates statistically significant difference from the WT value as determined by the Student's T-test (P < 0.05). (Adapted from Sivagurunathan et al., 2012; *Genetics*)

N.crassa movies for the WT and the mutant strains were also analyzed for the localization of FM 4-64 labeled vesicles inside the hyphae. For the WT and the mutant strains, it was observed that the vesicles accumulated more predominantly at the hyphal tip than in the hyphal body (Table 2). However, this vesicular accumulation pattern appeared to be altered in the p150Δ mutant strain and the reason is uncertain.

The overall motility analysis was separated based on the direction of the FM 4-64 labeled vesicles movements in the hyphae (Table 3). The vesicles that moved towards the hyphal tip were considered as the outward directed movements. And the vesicles that moved in towards the hyphal body were considered as the inward directed movements. Overall, I found no significant difference between the percentage of vesicles moving in the inward or outward direction for the WT and the DHC mutant. I observed that all the DHC mutant strains showed a significant decrease in the inward mean velocity, whereas for outward movements only some of the DHC mutant strains showed a decrease in the mean velocity. For the mean distances, I saw a significant decrease in the inward as well as outward directed movements in all the DHC mutant strains, except for Class 1 and Class 5.

From this work it is apparent that 1) DHC class mutations caused a severe and similar kind of transport defect that resulted in a significant decrease of various motility parameters; 2) the overall pattern of the transport defects observed in the DHC class mutants were comparable to that of DHCΔ mutant strain transport defects; and 3) if the *N. crassa* DHC class mutations would be generated in the mice, then these class mutations would cause severe transport defects and can lead to embryonic lethality similar to the DHCΔ mutation.

2.3.2 *N.crassa Loa* mutant results

The mouse neurodegenerative *Loa* mutation was generated in the *N. crassa* DHC to study the effect of this mutation on vesicular transport. The transport of FM 4-64 labeled vesicles in the growing hyphal tip of WT and *Loa* mutants were recorded using live cell imaging and the motility analysis was performed using kymographs.

2.3.2.1 Kymograph and motility analyses

Kymographs were plotted and analyzed to study the motility patterns of the FM 4-64 labeled vesicles in the WT and the mutant *Loa* hyphae.

Figure 17: Kymographs of the vesicles in the WT and mutant *Loa* hyphae

Kymographs (i.e. distance vs. time graphs) for various Wildtype (WT) and *Loa* mutant hyphae were generated. On a kymograph, the diagonal line (white arrow) represents a moving vesicle and the vertical line (black arrow) represents a stationary vesicle. (Adapted from Sivagurunathan et al., 2012; *Cytoskeleton*)

It can be seen from the kymographs that there were comparable number of diagonal lines in the WT as well as in the mutant *Loa* hyphae (Fig.17). This signifies that the WT and *Loa* hyphae have similar motility patterns. Data on run lengths, velocities and number of movements was generated for FM 4-64 labeled vesicles based on the *N. crassa* hyphae (WT and *Loa*) kymographs and is summarized in Table 4.

Table 4: Summary of motility analysis of WT and *Loa* strains

Summary of Vesicle Transport Dynamics		
	Wildtype	*Loa*
Motility index	24.6	26.9
Overall movements		
Mean movements/μm hyphal length	3.13	3.81
N	727	746
Inward movements		
Percent of total movements (%)	50.8	54.7
Mean velocity (μm/s ± SD)	1.66 ± 0.62	1.52 ± 0.66**
Mean distance (μm ± SD)	4.13 ± 2.24	3.88 ± 1.78
Outward movements		
Percent of total movements (%)	49.2	45.3
Mean velocity (μm/s ± SD)	1.78 ± 0.68	1.70 ± 0.60
Mean distance (μm ± SD)	4.47 ± 2.50	4.54 ± 2.08

**Statistically significant difference ($P < 0.001$) from wildtype value.

The motility index for the WT and the *Loa* mutant strain was similar to each other (Table 4) and it correlated with the comparable number of motility events as observed on their kymographs. The mean number of movements per micron hyphal length and the number of movements (*N*) did not show any reduction in the *Loa* mutant strain.

Both, the WT and the *Loa* mutant strain showed that the percentage of the inward directed vesicles was more than the outward directed vesicles (Table 4). In *Loa* mutant hyphae, I did not see any significant change in the mean distance (μm) of the inward or outward directed vesicles. However, I determined and statistically verified that there was a slight yet reproducible decrease in the mean velocity (μm/s) of inward directed vesicles in the *Loa* mutant hyphae as compared to the WT.

Lastly, it can be concluded that the *Loa* mutation did not cause a severe reduction in the motility parameters as previously seen in the 5 DHC class mutations of *N. crassa*. Nevertheless, the corresponding *Loa* mutation causes neurodegeneration in the *Loa* mutant mice. This implies that a mutation which results in a subtle transport defect is adequate enough to cause neurodegeneration. Furthermore, likelihood can be based on the observed *N. crassa* data and that is, a rigorous mutation like DHCΔ or any of the comparable 5 DHC class mutants would cause severe transport defects. It can be a possibility that severe transport defects might lead to death instead of causing neurodegeneration in the corresponding mutant organism.

2.4 Future directions

The *Loa* mutation did not cause a severe reduction in the motility parameters as previously seen in the 5 DHC class mutations of *N. crassa*. Hence, it can be determined that diverse *N. crassa* mutations (DHC class mutants and the *Loa* mutant) altered the intracellular motility but in different fashions. This indicates that these mutations do not utilize the same mechanism of action to affect dynein function.

In the future, it will be useful to study and understand the mechanism of how can these 5 DHC class mutations of *N. crassa* affect the dynein function as well as the intracellular transport in mice. For this purpose, one of the 5 DHC class mutations of *N. crassa* can be generated into a mice model. However, because these DHC class mutations are comparable to the DHCΔ mutation, it is most likely these DHC class mutations might cause embryonic lethality in the respective mutant mice model similarly to the DHCΔ mutant mouse model. Given the time and effort required to create a mutant mouse model, it would not seem worthwhile to create a mouse model which might be embryonic lethal.

Other future approaches can include generating DHC linked human neurodegenerative mutations in *N. crassa*. With all the given advantages of this fungi model system, it will be productive to study the effects of these neurodegenerative mutations on intracellular transport. If these mutant strains show subtle transport defects, then in support of it, our hypothesis can provide a possible mechanism of action of these neurodegenerative mutations.

CHAPTER 3: CAD CELLS MOTILITY ANALYSES

3.1 Introduction

Our long term goal is to study dynein and dynactin mutations in neurons. As a step in that direction, I utilized the mouse CAD cells for studying mitochondrial transport after impairing the dynein/dynactin motor complex.

3.2 Rationale for the approach

The CAD cell line is a mouse tissue culture cell system in which the cells were derived from a mouse brain tumor (Suri et al., 1993). These cells have synaptic vesicles and proteins similar to that found in neurons. When CAD cells are grown in a serum free medium, these cells extend out long projections that have resemblances to those in neurons (Fig.18) (Qi et al., 1997). Therefore, the CAD cell line can serve as an easy to use mammalian cell system to study long range transport.

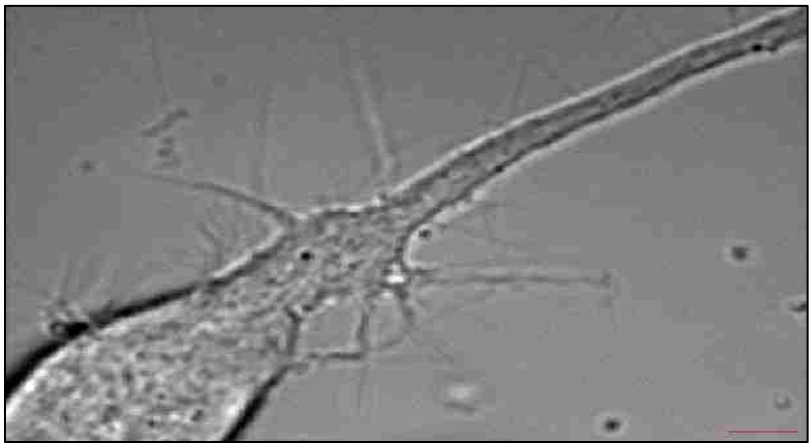

Figure 18: CAD cell in culture

CAD cells extend projections like neurons when grown in a serum free media. Scale bar = 5µm.

A recent study has shown that human neuropathy linked to DHC mutations may cause progressive mitochondrial dysfunction (Eschbach et al., 2013). Therefore, I decided to utilize mitochondria as a cargo to study the effects of dynein/dynactin motor protein complex impairments on intracellular transport in CAD cells. The mitochondria were visualized with an easy to use MitoTracker Green dye to track their motility during live cell imaging.

Two different approaches were applied to impair the dynein/dynactin motor complex: 1) Disrupting dynactin function with shRNA based approach and 2) inhibiting dynein function using a newly available drug Ciliobrevin (Firestone et al., 2012).

As descried in Chapter 1, the p150 subunit of dynactin binds and interacts with microtubules. shRNA technology was utilized to knock down the p150 subunit of dynactin in CAD cells. For a long term project goal, we wanted to study the effects on intracellular transport under the loss of function or reduction of dynactin levels (as caused by knockdown) and under the presence of neurodegeneration linked mutant dynactin (expressed exogenously) in CAD cells. Hence, we followed a "knockdown and replacement" strategy to support our future project goal (Fig.19). This two-step strategy was followed to avoid secondary effects of dynactin cable structure formation that are caused due to high amounts of dynactin inside the cell. Therefore, to maintain the normal level of dynactin inside the cell, endogenous p150 levels have to be reduced by knockdown and then replaced by the expression of exogenous mutant dynactin. Subsequent effect of exogenous expression of mutant dynactin on intracellular motility would be characterized to understand its mechanism of action.

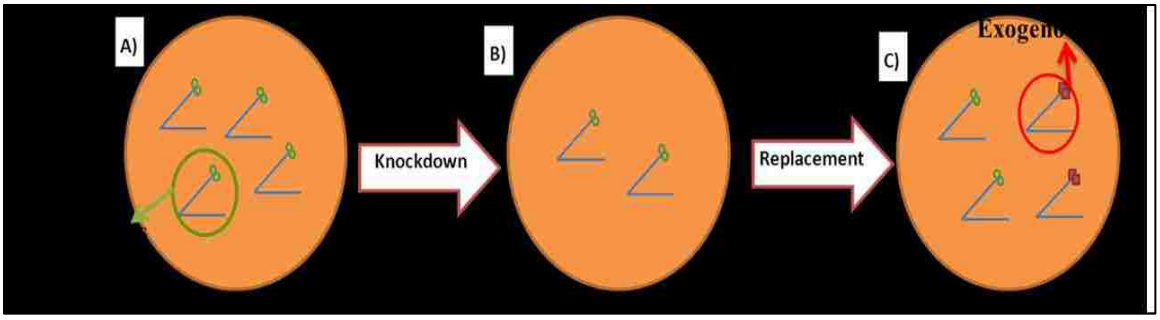

Figure 19: p150 subunit 'knockdown and replacement' strategy in CAD cells

Due to the p150 knockdown effect (A), the endogenous level of dynactin reduces in the cell (B). During the replacement step (C), a new p150 construct is expressed to generate new exogenous dynactin in the cell. (Blue p150 = endogenous dynactin. Red p150 = exogenous dynactin)

Alternate methods of disrupting dynactin function include overexpressing the CC-1 domain or the p50/dynamitin subunit of dynactin (Fig.20). Overexpression of the CC-1 domain causes that polypeptide to out-compete endogenous dynactin and bind to the dynein motor instead (King et al., 2003; Kwinter et al., 2009; Quintyne et al., 1999).

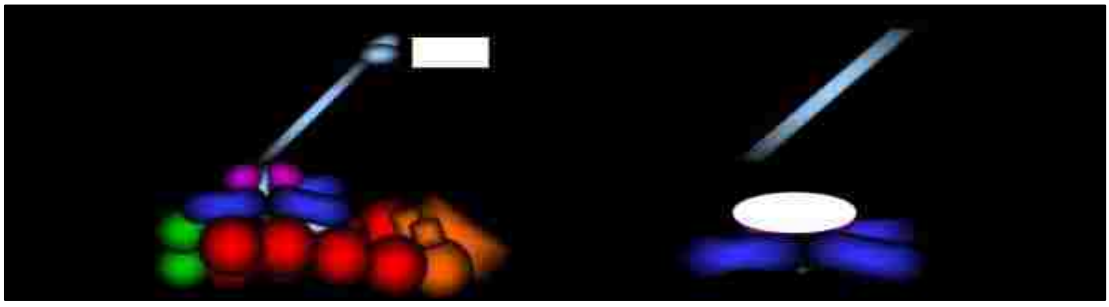

Figure 20: Other methods of disrupting dynactin function

Overexpression of the CC-1 domain or the p50/dynamitin subunits disrupts dynactin function inside the cells.

Overexpression of the p50/dynamitin subunit fragments the dynactin complex and disrupts its function (Echeverri et al., 1996; Eckley et al., 1999; Karki et al., 1998). These overexpression methods to disrupt dynactin function were not employed because they

would interfere with the abovementioned future goal of exogenously expressing neurodegeneration linked mutant dynactin and studying its effect.

The compound Ciliobrevin is a small molecular inhibitor of dynein. Ciliobrevin blocks the enzymatic activity of the AAA+ ATPase domains of dynein (Fig. 21). In this way Ciliobrevin is thought to inhibit the dynein motor *in vitro* and *in vivo* (Firestone et al., 2012). Hence, because of its specificity in action and ease of use, the Ciliobrevin drug was used to inhibit dynein function in my experiments.

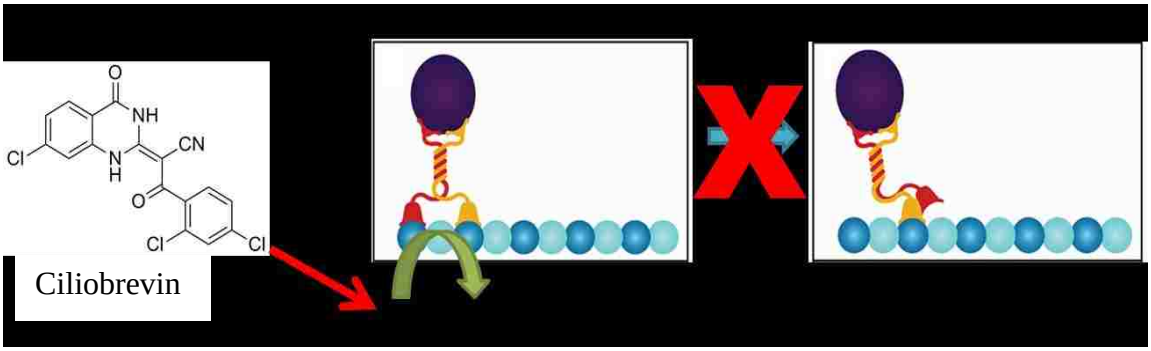

Figure 21: Ciliobrevin inhibits dynein's motor activity

Ciliobrevin is thought to block the enzymatic activity of the ATPase domains of the dynein motor. This result in the inhibition of dynein motor activity and dynein cannot move along a microtubule.

3.3 Background work: p150 knockdown quantification

For my motility experiments, it was critical to determine the extent of p150 knockdown from the shRNA approach. Unfortunately, we only had low percentage of transfected cells, so western blot analyses were not conclusive for determining p150 levels in transfected cells. However, the knockdown plasmid had another sequence encoding the red mCherry fluorescent protein to report which cells were transfected. Therefore, the King lab utilized immunofluorescence based approach to quantify the p150 knockdown in CAD cells.

For immunofluorescence staining experiment, the transfected CAD cells were fixed on a coverslip and immunostained with a primary antibody against the p150 subunit of dynactin and Alexa Fluor® 488 secondary antibody (Molecular Probes®) which fluoresced green. Images of view fields of cells containing both transfected (red signal) and untransfected (non red) cells were captured using our EMCCD camera. The fluorescence intensities of each cell were determined in both the red and green channels. The red channel gave the intensities of mCherry transfected cell and green channel gave the intensities of p150 indicating its level inside the cells.

From initial qualitative image assessment (Fig. 22), we could see that those cells which had sh p150 red fluorescent signal also had diminished green fluorescence signal. This implies that the red transfected cells on the sh p150 coverslip showed reduced amount of dynactin level due to knockdown. This was not observed for the control sh SCR transfected red cells. p150 levels in the sh SCR control cells were clearly not abolished although there was a clear reduction perceived by the eyes. We also noted that the Golgi apparatus maintained a tight phenotype in both control and p150 knockdown cells, indicating that we had not reduced the amount of dynactin to the point where Golgi fragmentation occurs (Holleran et al., 1998).

This qualitative screening was carried out for various time points i.e. 48h, 72h and 96h post transfection to check the maximum knockdown efficiency of sh p150 plasmid. It was determined that the best knockdown was achieved at 72h post transfection time point. Hence, later motility experiments were carried out in the cells at the 72h post transfection time point.

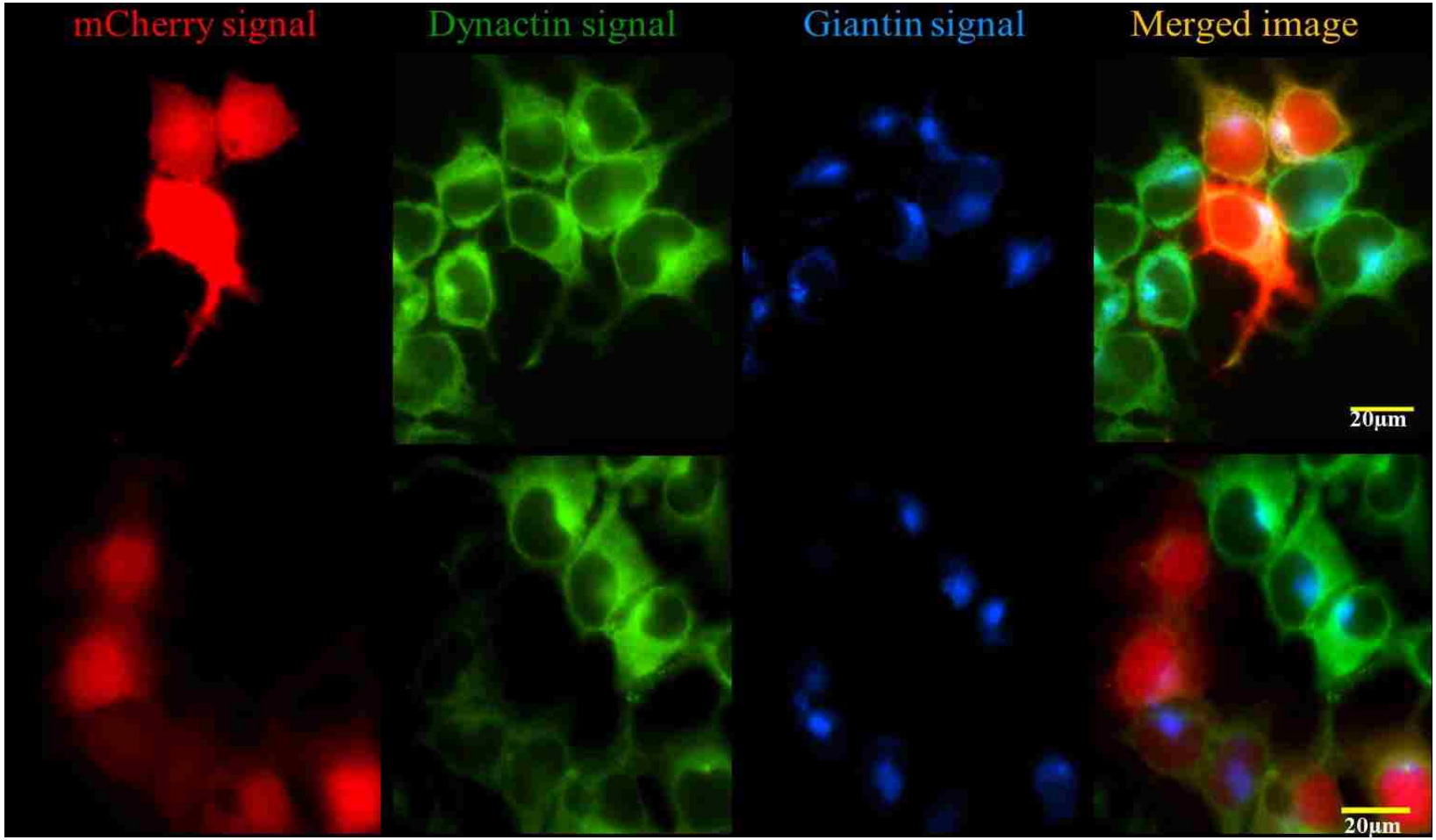

Figure 22: Immunostaining displaying p150 knockdown at 72 hrs

1st column-mCherry signal indicates transfected CAD cells; 2nd column- green p150 signal indicates level of p150 subunit; 3rd column- Giantin signal shows Golgi phenotype; 4th column- shows a merged image of all 3 channels. The sh p150 transfected red cells show a dimmer green intensity than untransfected and sh SCR red cells. (Data provided by Ranit Ghosh)

To quantitatively determine the knockdown efficiency, we determined the red and green fluorescence signals for each individual cell (Fig. 22). Then the data for each cell was plotted so that comparison can be made (Fig. 23). Each data point represented a single cell on the graph. The control cells (green data points) were untransfected 'no DNA' cells and these cells showed high levels of dynactin above 12,000 arbitrary units (au) on the y-axis. The sh SCR transfected cells (red data points) had high levels of dynactin above 10,000 au, independent of their mCherry red intensities (x-axis).

The sh p150 cells (blue data points) had two populations of transfected cells. First population contained those cells with red fluorescence below 10,000 au and these cells were either non-transfected (non red) or likely to be weakly transfected with no significant decrease in the p150 levels on y-axis. As seen from the inset image in Fig. 23, the control cell green data points basically show the background auto fluorescence of the cell at 1000 au red levels and in these cells level of p150 intensity was high. Similarly, the sh SCR and sh p150 cells with background auto fluorescence were at low red levels and showed high levels of p150 intensities.

The second population of sh p150 cells were noticeably transfected above the 10,000 au of red intensities. These truly transfected cells had reduced p150 levels as compared to the control and sh SCR cells, showing the knockdown effect of the sh p150 plasmid. Based on these results, a threshold line (shown in yellow) to determine the transfection was drawn at 10,000 au levels on x- axis. Hence, I performed my motility analyses only on cells with red intensities above 10,000 au, to ensure that these cells were truly transfected and the p150 knockdown effect has occurred in these cells.

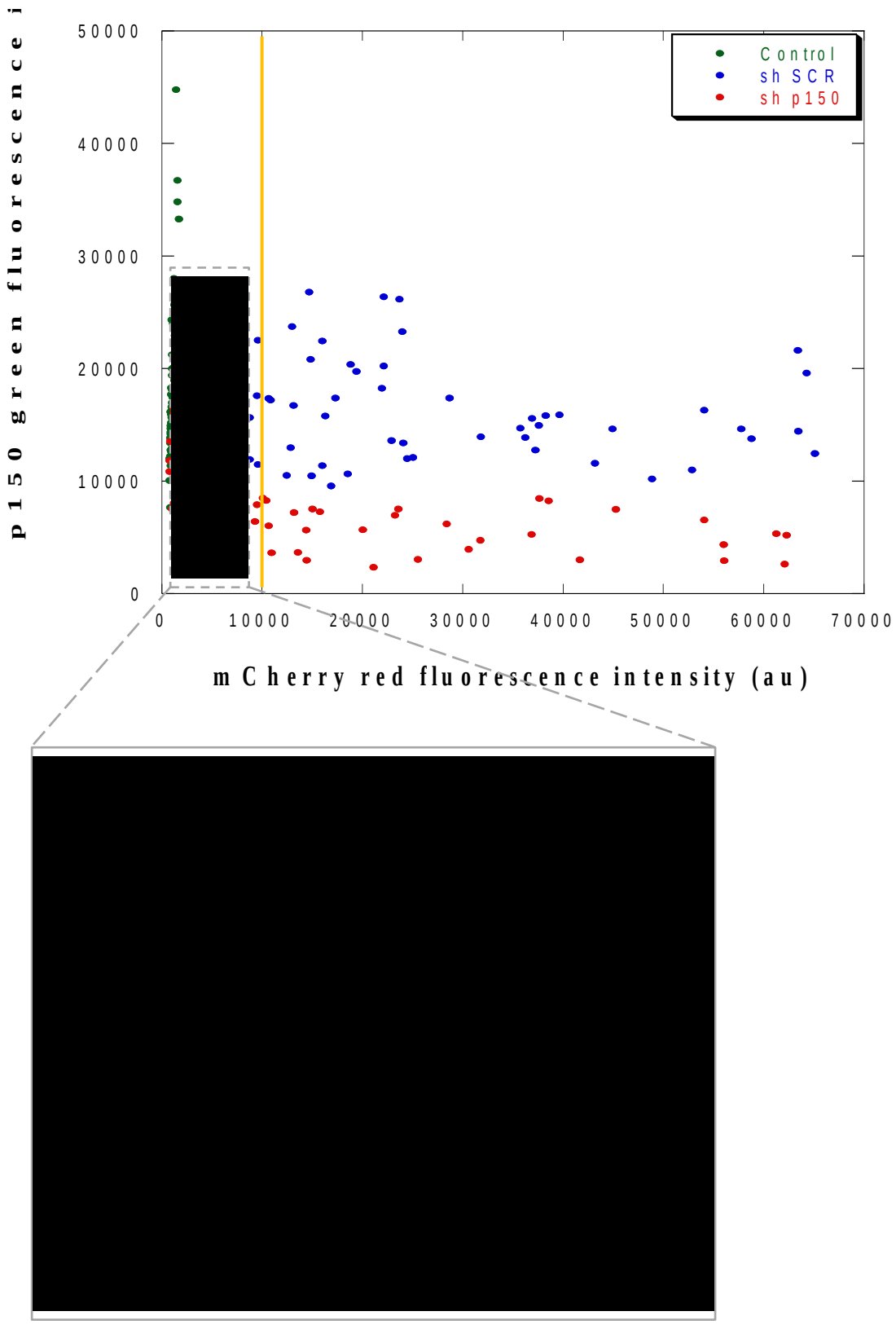

Figure 23: Quantification of p150 knockdown at 72 hrs

A graph was plotted between the red intensity of the transfected cells (x-axis) vs. green fluorescence intensity of dynactin level (y-axis). Each data point represents a single cell. The yellow line drawn at 10,000 au indicates a separation threshold point between the two populations of cells as described in the text. (Data provided by Ranit Ghosh).

3.4 Results and discussion

3.4.1 Effects of dynactin disruption on motility

To study the effects of dynactin disruption on the mitochondrial motility, live cell imaging for motility events were recorded from different portions on coverslip and the imaging experiments was repeated on three different days. From the collected data of live cell movies, I picked up cells that had red fluorescent intensities more than 10,000 au for truly sh p150 and sh SCR transfected cell. In these movies, I observed that more number of mitochondria were actively transported in the WT and sh SCR control cells than in the sh p150 knockdown cells.

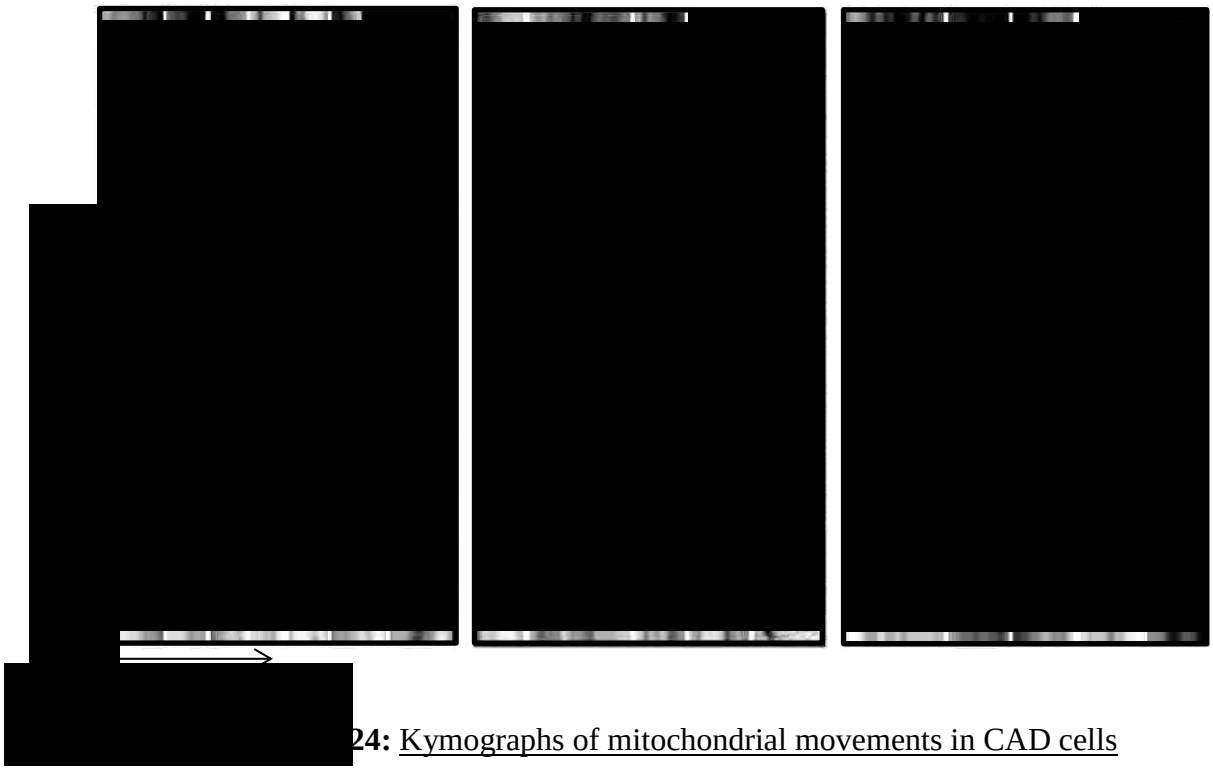

24: Kymographs of mitochondrial movements in CAD cells

The control Wildtype (WT) and sh SCR kymographs show more diagonal lines than the sh p150 knockdown kymograph. Because each diagonal line represents a motility event, therefore there was less motility events observed in sh p150 knockdown cells. (Distance on x-axis and time on y-axis)

From respective live cell movies, kymographs (Fig. 24) were generated for the WT, sh SCR control and sh p150 knockdown cells. The kymograph for WT cell showed several diagonal lines indicating high number of motility events. The sh SCR kymograph was comparable to the WT kymographs with lot of motility events. The kymograph for the sh p150 knockdown cell had lesser number of diagonal lines than the WT implying that less motility events happened in the sh p150 knockdown cell.

Table 5: Mitochondrial motility data in CAD cells

	WT Control cells	sh SCR Transfected cells	sh p150 Transfected cells
Total movements (n)	644	347	172
Average number of movements/cell	65	66	25 *
Average Velocity (µ/s)	0.78 ± 0.4	0.86 ± 0.4	0.83 ± 0.4
Average Distance (µ)	0.94 ± 0.7	1.04 ± 0.7	1.30 ± 1.0 *

The table shows mitochondrial motility data for control cells Wildtype (WT), sh SCR and for the sh p150 knockdown cells. The data was collected at 72hr post transfection time point. The '*' indicates values that were significantly different from the control values, $P < 0.01$ (Student's T-test).

From the kymographs of movies from each condition, I was able to determine the direction, run length and velocities of each motility event as well as the total number of movements (Table 5). When compared to the control cells, I found that the average number of mitochondrial movements per cell was significantly reduced in the sh p150 knockdown cells. Because p150 knockdown cells also have reduced dynactin present (Fig. 23), it appears most likely that p150 has a normal role in helping with mitochondrial movements by functioning as a dynein cargo adaptor and linking dynein to the

mitochondria for transport. No significant change was noted in the average velocity of mitochondrial movements between the control and the knockdown cells.

However, I observed an unexpected increase in the average distance travelled by the mitochondria in the sh p150 knockdown cells. This was unexpected because dynactin has been identified as a processivity enhancer for dynein (Culver-Hanlon et al., 2006) and under that model, the loss of dynactin should have lowered the distance mitochondria travelled in each motility event. One possibility to explain this discrepancy is that dynactin disruption in the knockdown cells might have changed the state where kinesin and dynein were equally active to a state where kinesin is predominantly more active. This might have altered the active kinesin vs. active dynein ratio and may have decreased the number of "tug-of-war" situations between the opposite ended motor proteins (as mentioned in the Introduction chapter). Because of the loss of active dynein, kinesin may have been then able to run uninhibited for longer distances and resulted in longer mitochondrial run lengths as observed in the p150 knockdown cell. An analogy that can be used to understand this behavior is a classic 'tug-of-war' game with two teams pulling on a single rope (mitochondria). When one team (dynein) has less active members (due to p150 knockdown), then the other team (kinesin) is more likely to move unopposed as it is significantly stronger than the other weakened team (dynein).

The data observations became much clearer when the data points for each mitochondrial movement were plotted in a distance (x-axis) vs. velocity (y-axis) graph (Fig, 25). The WT and sh p150 data points were each clustered for the most part at the short distances side i.e. on the left area of the graph. Interestingly, I observed that the mitochondrial movements at longer distances were predominantly of sh p150 knockdown

cells (circled in Fig. 25). This observation correlates with the significant increase found in the average distances of sh p150 mitochondrial movements as seen in the Table 5.

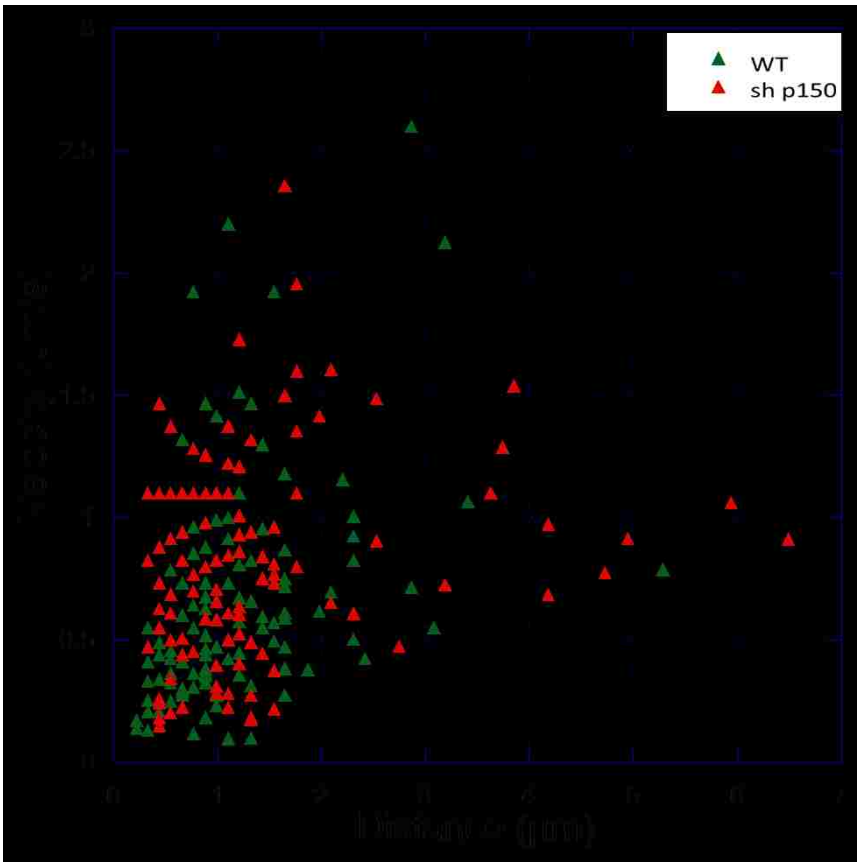

Figure 25: Distance vs. Velocity graph of mitochondrial movements

WT and sh p150 motility events are plotted with distance on x-axis and velocity on y-axis. A subset of circle data points (encircled) represent the longest run lengths for the mitochondrial movements.

Next, the mitochondrial movements were plotted in a histogram (Fig. 26) of the percentage of movements (y-axis) per µm distance intervals (x-axis). I noted that about 70% of WT mitochondrial movements occurred at shorter distance of ~1µm. For the sh p150 knockdown cells, only 50% mitochondrial movements occurred at shorter distances under ~1µm. Additionally, for the sh p150 knockdown cells, I saw a corresponding shift in the percentage of mitochondrial movements to the longer distance bin intervals

(>1µm) compared to the WT mitochondrial movements. Exponential curve fitting of the histogram bar graph provided a rationale for the behavior I observed. For WT cells a simple exponential decay provides an excellent fit to the data with the best correlation factor (R) for the curve equations, indicating that a single uniform probability event governs the distance mitochondria moved. Based on the large literature supporting single exponential decay fits for single motors, it appear that the WT mitochondria are moved by a single motor in CAD cells.

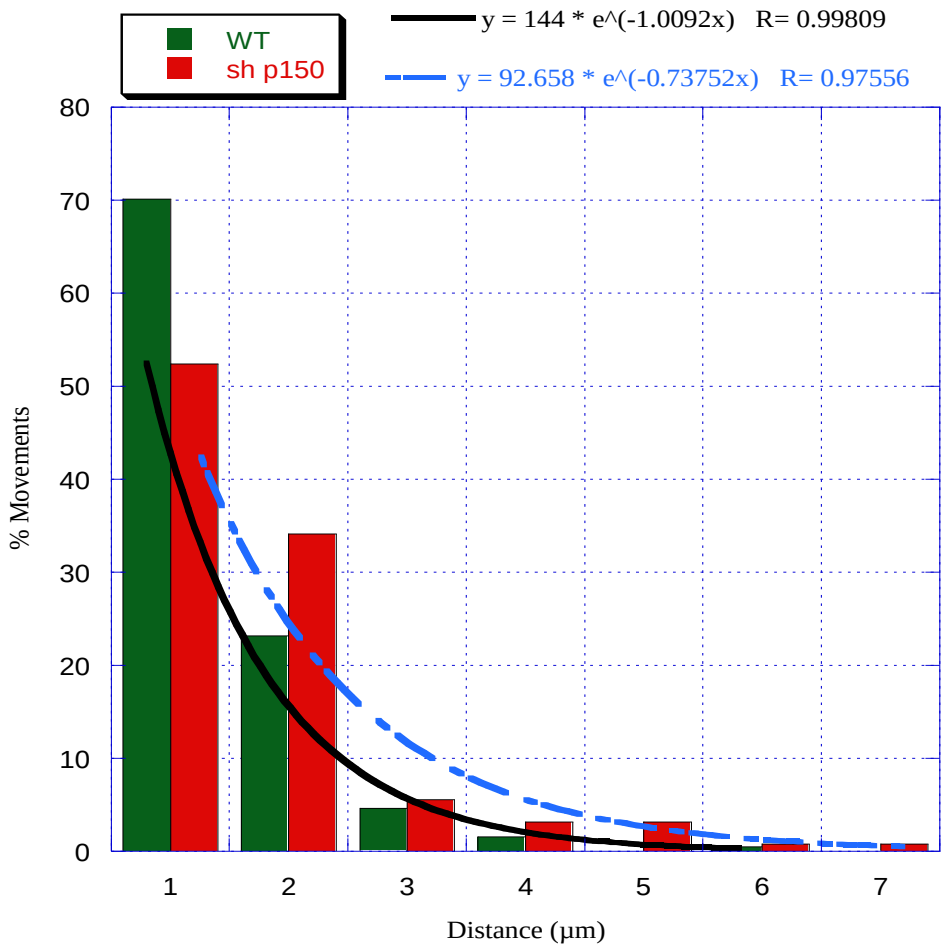

Figure 26: Histogram of percentage of mitochondrial movements

The plot shows the distribution of mitochondrial movements in one micron (µm) distance intervals. WT and sh p150 data can be fit to single exponential decay curves (black for WT; blue for sh p150), with the WT data providing a stronger fit than the sh p150 data (as determined by the 'correlation factor' R).

In contrast, the curve is clearly shifted in sh p150 cells and an exponential decay does not fit the observed data as well as for the WT cells. This indicates that some additional factors besides a single active motor, are acting on mitochondrial distance travelled in p150 knockdown cells. Also, the correlation curve equation explains that compared to the WT cell, the mitochondrial movements in sh p150 knockdown cells perpetuated longer before disassociating (or decaying) from the microtubule. Hence, this supports the observation of the longer mitochondrial run lengths obtained in the sh p150 knockdown cells.

3.4.2 Effects of dynein inhibition on motility

Ciliobrevin has the potential to be on an incredibly powerful tool for motility studies as it inhibits dynein motor activity *in vitro* and *in vivo* (Firestone et al., 2012). I decided to utilize this drug as a way to inhibit dynein in CAD cells and record live cell movies showing its effect on the mitochondrial motility. There were two clear consequences of adding the Ciliobrevin in CAD cells. The first and expected consequence was that the mitochondrial motility dropped significantly after adding the drug. Live cell movies provided data that was not suitable for generating kymographs and hence, further analysis using motility counts was performed. Cells treated with Ciliobrevin showed an average number of movements close to 15, which was lesser than the average number of movements of 50 in an untreated control cell. The second and totally unexpected consequence of Ciliobrevin addition was an immediate change in the morphology of vast majority of mitochondria in CAD cells.

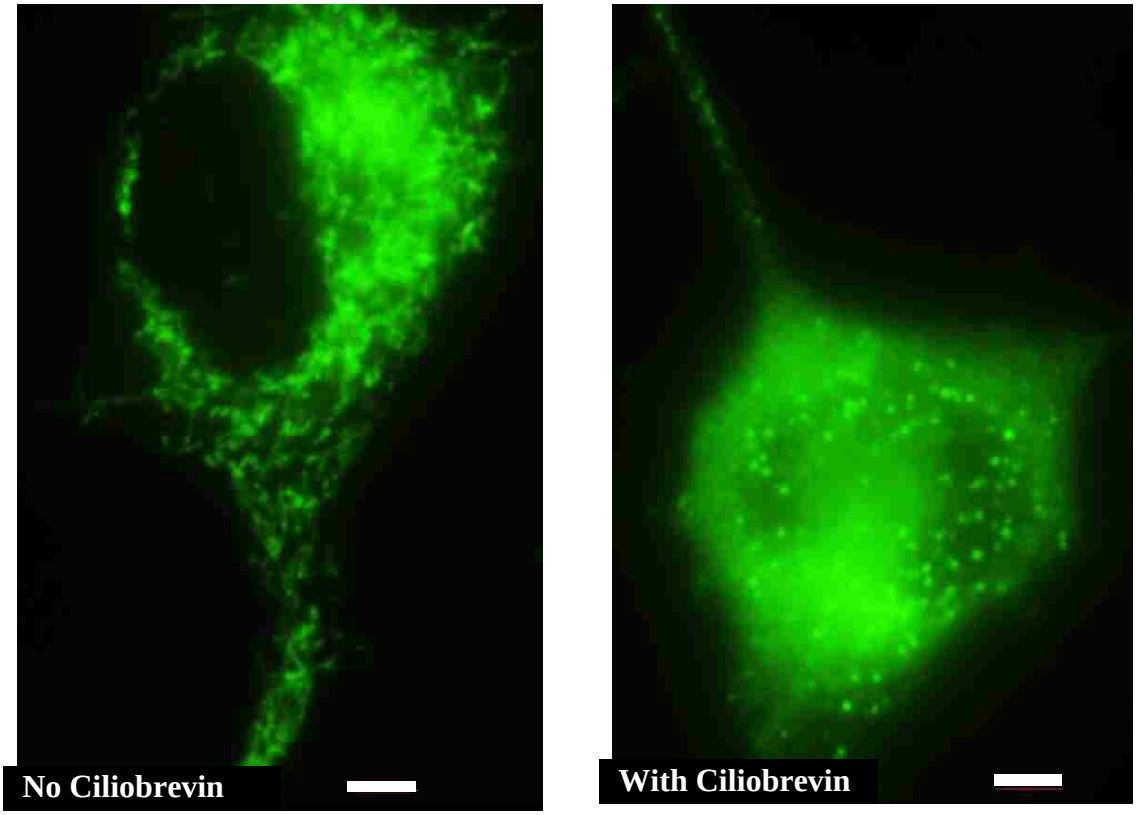

Figure 27: Effect of Ciliobrevin on mitochondrial motility

CAD cells with mitochondria labeled using MitoTracker® Green fluorescent dye. Left: a control cell with no drug added in which mitochondrial morphology looked normal. Right: a cell with Ciliobrevin drug (100μM) added in which the mitochondrial morphology changed significantly. Scale bar = 5μm.

Normally mitochondria are long and stretched out with cigar like shape, however, after addition of Ciliobrevin mitochondria rounded up into what appear to be larger spheres (Fig. 27). Future experiments will be required to further characterize the mitochondrial morphology change.

The unexpected mitochondrial morphology change raises a serious concern on the specificity of Ciliobrevin drug in inhibiting the dynein motor function. It is unclear if the drop in mitochondrial motility was caused by the mitochondrial morphology change. Alternatively, the reverse can be possible: the mitochondria change in morphology could

be caused by a drop in dynein motility. This second possibility could be due to some process where active dynein motors are needed to maintain mitochondria shape. However, treatments with microtubule polymerizing drugs (such as nocodazole) that prevent dynein activity do not cause such morphology change (Kabashima et al., 2013). Another possibility could be that both the events (mitochondrial morphology change and motility drop) can occur independent to each other. For example, Ciliobrevin may inhibit dynein motor as expected, yet also directly inhibit some other critical ATP sensitive protein that plays an important role in maintaining the mitochondrial morphology.

Hence, due to the non-specific inhibitory effects caused on the mitochondria in the cells, Ciliobrevin appears to be a "troublesome" inhibitor. In light of my observation with Ciliobrevin, I will not prefer to inhibit dynein function with this approach in future experiments.

3.5 Future directions

I determined that affecting any one component of the dynein/dynactin motor complex does affect the intracellular motility, but in different fashion. In p150 knockdown cells, the effect of partial loss of dynactin function was observed as a decrease in the average number of mitochondrial movements and an increase in the mitochondrial run length was seen.

The ground work is now set to carry out the second step of the 'knockdown and replacement' strategy involved in the long term future goal of reducing the endogenous dynactin level and expressing an exogenous neurodegeneration linked mutant dynactin. It would be exciting to see how the mitochondrial motility of the cell is affected by the

exogenous expression of neurodegenerative-linked mutant dynactin. One possibility is that mutant dynactin can rescue motility defects by increasing the average number of mitochondrial movements in a p150 knockdown-replaced cell. This means that, instead of causing transport defects, the mutation in dynactin has a different mechanism of causing neurodegeneration. For example, in this case the mutation might be causing dynactin to misfold and hence leading to neurodegeneration, even though there is no transport defect as it was seen in a dynactin knockdown cell. Alternatively, the mutant dynactin can drastically alter the mitochondrial motility parameters in the p150 knockdown-replaced cells. This would imply that mutations in dynactin lead to transport defects and this can be directly linked as a mechanism for causing neurodegeneration by such dynactin mutations.

CHAPTER 4: MATERIALS AND METHODS

4.1 *N.crassa* motility analyses

4.1.1 Vesicle labeling

N. crassa hyphae were treated with the membrane binding dye called FM® 4-64 [N-(3-Triethylammoniumpropyl)-4-(6-(4-(Diethylamino) Phenyl) Hexatrienyl) Pyridinium Dibromide, (Molecular Probes®, Invitrogen™)]. This dye stains lipid membranous vesicles and fluoresces red under proper excitation wavelength on a fluorescent microscope. The following steps were followed to label the vesicles with FM4-64 dye:

1. The *N.crassa* strains (WT and various mutant strains) were grown on a VSM agar (Vogel's minimal media + 2% Sucrose) coated slide and incubated at 28°C for 16-18 hrs.
2. FM 4-64 dye (5µM final concentration) was mixed with VSM liquid medium and about 20µl was added to the VSM coated slide containing growing hyphae.
3. A coverslip was added on top of the VSM liquid followed by immediate visualization (live cell imaging) on a microscope.

4.1.2 Live cell imaging

The microscope used for the *N. crassa* live cell imaging was an Olympus BX50 upright microscope with a 100X (1.3 N.A.) oil immersion objective lens. The movies were acquired using SPOT software (v3.5.9) on a SPOT RT-SE 18 camera system (Diagnostic Instruments). Each time-lapse live cell movie was made with images taken every 200 millisecond for a total duration of 30 seconds. A movie stack was comprised of

150 frames as five frames were taken per second. Each pixel of the image was 0.13 µm across at the magnification used. Between 10 and 15 movies tracking the FM 4-64 stained vesicles were captured for the *N.crassa* WT and DHC mutant strains.

4.2 CAD cell motility analyses

4.2.1 Cell Culture

CAD cells were grown in a T75 tissue culture flask with complete CAD medium containing DMEM/F12 Nutrient Mix (Gibco®) with Glutamax™ (1%,Gibco®), Pen/Strep (1%) and Fetal Bovine Serum (FBS, 10%). Next, the cells were plated from a T75 flask onto a 25mm coverslip (10,000-15,000 cell density) in a six well plate. These plated cells were then grown in a FBS free medium so that they extend projections.

4.2.2 Transfection with knockdown plasmid

To knockdown the endogenous level of dynactin in CAD cells, the short hairpin (sh) plasmids against the external region (3'UTR) of the p150 coding sequence (sh p150) were used.

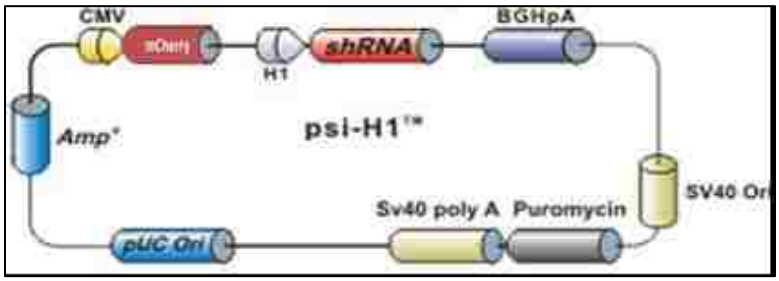

Figure 28: Knockdown sh-plasmid structure

The knockdown sh plasmid has a shRNA coding sequence against the p150 subunit or a scrambled coding sequence for transfection control. The shRNA region is under the control of the H1 promoter. The sh plasmid also has a coding sequence for the mCherry red fluorescent protein (under the CMV promoter) to indicate transfected cells.

For transfection controls, sh plasmids containing a scrambled coding sequence (sh SCR) were used. The shRNA expression was under the control H1 promoter (Fig. 28) and the plasmid also contained a coding sequence to produce the red fluorescent protein mCherry as a reporter signal to indicate transfected cells.

For the knockdown experiments, the CAD cell coverslips were transfected 24 hours after plating onto coverslips. The CAD cells were either transfected with a sh p150 or with a control sh SCR plasmid.

The following steps were followed for the transfection-

1. For each coverslip, 100µl of Opti-MEM® reduced serum (Gibco®) was mixed with 6µl of X-tremeGENE HP DNA Transfection Reagent (Roche) in a tube and incubated for 10 minutes.
2. Next, sh p150 or sh SCR plasmid DNA (2µg/coverslip) was added to the tube and incubated for 15 minutes.
3. After the incubation was complete, the plasmid DNA mix was added to 2ml of FBS free CAD medium and gently mixed.
4. The old media was removed from the well containing CAD cells on a coverslip, and then the plasmid DNA mix was added. The cells were incubated overnight at 37°C in a standard humidified CO_2 incubator.
5. The next morning, the media over the coverslip was replaced with 2ml of fresh FBS free CAD medium.

4.2.3 Mitochondria labeling

MitoTracker® Green (Molecular Probes®, Invitrogen™) was used to label and track mitochondria in CAD cells. The mitochondria labeling steps were as follow:

1. Media was removed from a well containing a coverslip and the CAD cells were gently rinsed with ~ 1.5 ml PBS (0.01 M phosphate buffer, 0.0027 M KCl and 0.137 M NaCl, Sigma).
2. After removing the PBS, freshly prepared 1ml of MitoTracker Green (50nM) in FBS free CAD media was added and incubated at 37°C for 30 minutes.
3. After the incubation, the MitoTracker Green containing media was removed from the coverslip and the cells were again gently rinsed with ~1.5ml PBS.
4. The coverslip was removed from the well and placed in a pre-warmed live cell chamber.
5. Warm 1.5ml FBS free CAD media was added gently on to the cells and a fresh coverslip was put on top to prepare a live cell chamber for imaging.

4.2.4 Ciliobrevin treatment

CAD cells were treated with a 100µM Ciliobrevin drug (Trade name: Calbiochem, EMD Millipore) to inhibit dynein function. A Ciliobrevin stock solution (10mM) was prepared in DMSO. Ciliobrevin drug treatment steps were as follows:

1. Media was removed from CAD cells and the cells were gently rinsed with ~ 1.5 ml PBS.

2. After removing the PBS, freshly made 1ml of the 50nM MitoTracker Green dilution with FBS free CAD media was added and incubated at 37°C for 30 minutes.
3. After the incubation period, the MitoTracker Green solution was removed from the coverslip and the cells were again gently rinsed with ~1.5ml PBS.
4. The coverslip was removed from the well and placed in a pre-warmed live cell chamber.
5. Warm 1.5ml FBS free CAD media with 15µl of Ciliobrevin stock solution (10mM) was added gently on to the cells.
6. A fresh coverslip was put on top to prepare the live cell chamber of CAD cells for imaging.

4.2.5 Live cell imaging

The mitochondrial motility movies were acquired by the 'stream acquisition' function of the Metamorph software (Molecular Devices, CA) using an Evolve™ 512 EMCCD camera (Photometrics® System). The microscope used was a Nikon® Eclipse T*i* inverted fluorescent microscope with a CFI Apo TIRF 100X/1.49 oil immersion objective lens with an additional 1.5X magnification adaptor. Each live cell movie prepared was a stack of 500 frames, with 10 frames taken per second for a total duration of 50 seconds. Each pixel of the image was 0.11 µm across at the magnification used. Numerous movies of mitochondrial motility under the p150 knockdown and control conditions were recorded and repeated at least on three separate days.

4.3 Kymograph and data analyses

The analysis of live cell motility movies for *N. crassa* and CAD cells were carried out using Metamorph Software (Molecular Devices, CA). On a movie frame (Fig. 29 I), a region line 'A to B' was drawn to track the path of the moving cargoes (FM® 4-64 labeled vesicles or mitochondria). The region line 'AB' was then generated into a kymograph (Fig. 29 II). A kymograph is a distance (x-axis) vs. time (y-axis) graph that showed the position of all fluorescent signals (cargo) during the course of the movie. So, if there is a cargo that did not move during the course of the movie, then a vertical line (Fig.29 II, blue line) was generated on a kymograph representing that cargo's stationary motility pattern. That vertical line had a constant distance that did not change with time on the kymograph. However, if a cargo moved, then the fluorescent signal generated a diagonal line (Fig.29 II, yellow line) that showed a distance displacement with respect to time. Hence, the vertical lines on the kymographs represented the stationary cargoes and the diagonal lines with slopes represented the moving cargoes.

Next, I performed further analyses to obtain data on diagonal lines from the kymographs (Fig. 29 III). The width (in pixels) of the diagonal lines was measured from the kymograph and entered in a customized excel sheet. The excel sheet had formulae based on the pixels/µm value of the microscope to generate the respective real distance (in µm) of the cargo. Similarly, the height (in pixels) of the diagonal lines was measured and gave a value of the real time duration (in seconds) in the excel sheet. The real distance (µm) was divided by the real time (seconds) to generate the real velocities (µm/seconds) of the cargo.

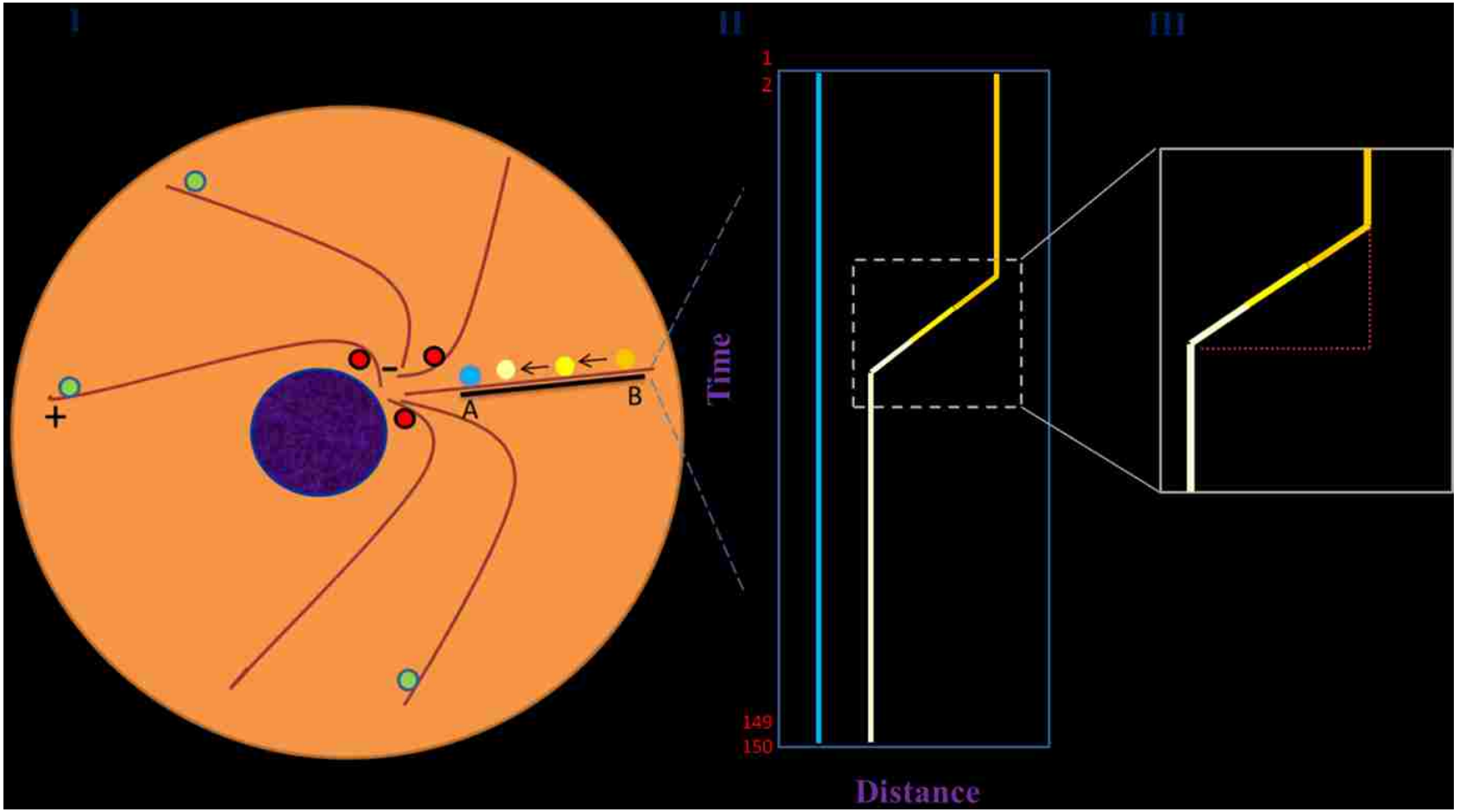

Figure 29: Kymograph generation and analysis

Panel I: A region line 'AB' is drawn on a movie frame to track the movement of cargo (blue and yellow circles). Panel II: Kymograph (distance vs. time graph) is generated from the region line 'AB'. The blue vertical line represents stationary cargo and the yellow line represents stationary-movement-stationary motility pattern of a moving cargo. Panel III: The height, width and slope of the diagonal line can give information on the time duration (seconds), distance (µm) and the velocity (µm/sec) of the moving cargo.

Also, the angle of the slope provided information on the direction of the cargo movements. The angle specified if the cargo was moving from the cell center to the cell periphery or vice versa. This slope determination helped in generating the percentage of movements happening in the inward vs. outward directions.

Also, the growth rate of *N. crassa* hyphal tip was calculated by measuring the starting point of the tip (in pixels) at the beginning of the movie and the final point of the grown tip at the end of the movie. Next, these distances were converted to real distances (in µm) and the distance of the initial hyphal tip length was subtracted for the final hyphal tip length. The length difference (in µm) was divided by the duration of the movie that is 30 seconds to get the rate of growth (µm/seconds) of the hyphal tip.

REFERENCES

- Baloh, R., M. Harms, K. Ori-McKenney, M. Scoto, E. Tuck, S. Bell, D.D. Ma, S. Masi, P. Allred, M. Al-Lozi, M. Reilly, L. Miller, A. Jani-Acsadi, A. Pestronk, M. Shy, F. Muntoni, and R. Vallee. 2012. Mutations in the Tail Domain of DYNC1H1 Cause Dominant Spinal Muscular Atrophy. *Neurology*. 78.

- Banks, G.T., and E.M. Fisher. 2008. Cytoplasmic dynein could be key to understanding neurodegeneration. *Genome Biol*. 9:214.

- Burgess, S.A., M.L. Walker, H. Sakakibara, K. Oiwa, and P.J. Knight. 2004. The structure of dynein-c by negative stain electron microscopy. *J Struct Biol*. 146:205-216.

- Burkhardt, J.K., C.J. Echeverri, T. Nilsson, and R.B. Vallee. 1997. Overexpression of the dynamitin (p50) subunit of the dynactin complex disrupts dynein-dependent maintenance of membrane organelle distribution. *J Cell Biol*. 139:469-484.

- Carter, A.P., C. Cho, L. Jin, and R.D. Vale. 2011. Crystal structure of the dynein motor domain. *Science*. 331:1159-1165.

- Chen, X.J., E.N. Levedakou, K.J. Millen, R.L. Wollmann, B. Soliven, and B. Popko. 2007. Proprioceptive sensory neuropathy in mice with a mutation in the cytoplasmic Dynein heavy chain 1 gene. *J Neurosci*. 27:14515-14524.

- Chevalier-Larsen, E.S., K.E. Wallace, C.R. Pennise, and E.L. Holzbaur. 2008. Lysosomal proliferation and distal degeneration in motor neurons expressing the G59S mutation in the p150Glued subunit of dynactin. *Human molecular genetics*. 17:1946-1955.

- Culver-Hanlon, T.L., S.A. Lex, A.D. Stephens, N.J. Quintyne, and S.J. King. 2006. A microtubule-binding domain in dynactin increases dynein processivity by skating along microtubules. *Nat Cell Biol*. 8:264-270.

- Dick, T., K. Ray, H.K. Salz, and W. Chia. 1996. Cytoplasmic dynein (ddlc1) mutations cause morphogenetic defects and apoptotic cell death in Drosophila melanogaster. *Mol. Cell Biol.* 16:1966-1977.

- Duchen, L.W. 1974. A dominant hereditary sensory disorder in the mouse with deficiency of muscle spindles: the mutant Sprawling. *J Physiol*. 237:10P-11P.

- Dujardin, D., U.I. Wacker, A. Moreau, T.A. Schroer, J.E. Rickard, and J.R. De Mey. 1998. Evidence for a role of CLIP-170 in the establishment of metaphase chromosome alignment. *J Cell Biol*. 141:849-862.
- Echeverri, C.J., B.M. Paschal, K.T. Vaughan, and R.B. Vallee. 1996. Molecular characterization of the 50-kD subunit of dynactin reveals function for the complex in chromosome alignment and spindle organization during mitosis. *J Cell Biol*. 132:617-633.

- Eckley, D.M., S.R. Gill, K.A. Melkonian, J.B. Bingham, H.V. Goodson, J.E. Heuser, and T.A. Schroer. 1999. Analysis of dynactin subcomplexes reveals a novel actin-related protein associated with the arp1 minifilament pointed end. *J Cell Biol*. 147:307-320.

- Eschbach, J., J. Sinniger, J. Bouitbir, A. Fergani, A.I. Schlagowski, J. Zoll, B. Geny, F. Rene, Y. Larmet, V. Marion, R.H. Baloh, M.B. Harms, M.E. Shy, N. Messadeq, P. Weydt, J.P. Loeffler, A.C. Ludolph, and L. Dupuis. 2013. Dynein mutations associated with hereditary motor neuropathies impair mitochondrial morphology and function with age. *Neurobiol Dis*.

- Farrer, M.J., M.M. Hulihan, J.M. Kachergus, J.C. Dachsel, A.J. Stoessl, L.L. Grantier, S. Calne, D.B. Calne, B. Lechevalier, F. Chapon, Y. Tsuboi, T. Yamada, L. Gutmann, B. Elibol, K.P. Bhatia, C. Wider, C. Vilarino-Guell, O.A. Ross, L.A. Brown, M. Castanedes-Casey, D.W. Dickson, and Z.K. Wszolek. 2009. DCTN1 mutations in Perry syndrome. *Nat Genet*. 41:163-165.

- Firestone, A.J., J.S. Weinger, M. Maldonado, K. Barlan, L.D. Langston, M. O'Donnell, V.I. Gelfand, T.M. Kapoor, and J.K. Chen. 2012. Small-molecule inhibitors of the AAA+ ATPase motor cytoplasmic dynein. *Nature*. 484:125-129.

- Gennerich, A., and R.D. Vale. 2009. Walking the walk: how kinesin and dynein coordinate their steps. *Current opinion in cell biology*. 21:59-67.

- Gibbons, I.R., B.H. Gibbons, G. Mocz, and D.J. Asai. 1991. Multiple nucleotide-binding sites in the sequence of dynein β heavy chain. *Nature*. 352:640-643.

- Gibbons, I.R., A. Lee-Eiford, G. Mocz, C.A. Phillipson, W.-J.Y. Tang, and B.H. Gibbons. 1987. Photosensitized cleavage of dynein heavy chains. *J. Biol. Chem.* 262:2780-2786.

- Hafezparast, M., R. Klocke, C. Ruhrberg, A. Marquardt, A. Ahmad-Annuar, S. Bowen, G. Lalli, A.S. Witherden, H. Hummerich, S. Nicholson, P.J. Morgan, R. Oozageer, J.V. Priestley, S. Averill, V.R. King, S. Ball, J. Peters, T. Toda, A. Yamamoto, Y. Hiraoka, M. Augustin, D. Korthaus, S. Wattler, P. Wabnitz, C. Dickneite, S. Lampel, F. Boehme, G. Peraus, A. Popp, M. Rudelius, J. Schlegel, H. Fuchs, M. Hrabe de Angelis, G. Schiavo, D.T. Shima, A.P. Russ, G. Stumm, J.E. Martin, and E.M. Fisher. 2003. Mutations in dynein link motor neuron degeneration to defects in retrograde transport. *Science*. 300:808-812.
- Harada, A., Y. Takei, Y. Kanai, Y. Tanaka, S. Nonaka, and N. Hirokawa. 1998. Golgi vesiculation and lysosome dispersion in cells lacking cytoplasmic dynein. *J. Cell Biol.* 141:51-59.

- Holleran, E.A., S. Karki, and E.L. Holzbaur. 1998. The role of the dynactin complex in intracellular motility. *Int Rev Cytol*. 182:69-109.

- Holleran, E.A., L.A. Ligon, M. Tokito, M.C. Stankewich, J.S. Morrow, and E.L.F. Holzbaur. 2001. Beta III spectrin binds to the Arp1 subunit of dynactin. *J. Biol. Chem.* 276:36598-36605.

- Hoogenraad, C.C., A. Akhmanova, S.A. Howell, B.R. Dortland, C.I. De Zeeuw, R. Willemsen, P. Visser, F. Grosveld, and N. Galjart. 2001. Mammalian Golgi-associated Bicaudal-D2 functions in the dynein-dynactin pathway by interacting with these complexes. *Embo J*. 20:4041-4054.

- Kabashima, K., D. Yoshinaga, J. Fang, M. Matsuzaki, and H. Suzuki. 2013. Cell cycle-dependent dynamics of cytoskeleton involving mitochondrial redistribution in hamster embryos. *Reproduction in domestic animals = Zuchthygiene*. 48:267-271.

- Karki, S., B. LaMonte, and E.L. Holzbaur. 1998. Characterization of the p22 subunit of dynactin reveals the localization of cytoplasmic dynein and dynactin to the midbody of dividing cells. *J Cell Biol*. 142:1023-1034.

- Kincaid, M.M., and S.J. King. 2006. Motors and their tethers: the role of secondary binding sites in processive motility. *Cell Cycle*. 5:2733-2737.

- King, S.J., M. Bonilla, M.E. Rodgers, and T.A. Schroer. 2002. Subunit organization in cytoplasmic dynein subcomplexes. *Protein Sci*. 11:1239-1250.

- King, S.J., C.L. Brown, K.C. Maier, N.J. Quintyne, and T.A. Schroer. 2003. Analysis of the dynein-dynactin interaction in vitro and in vivo. *Mol Biol Cell*. 14:5089-5097.

- King, S.J., and T.A. Schroer. 2000. Dynactin increases the processivity of the cytoplasmic dynein motor. *Nat Cell Biol*. 2:20-24.

- Kon, T., K. Sutoh, and G. Kurisu. 2011. X-ray structure of a functional full-length dynein motor domain. *Nat Struct Mol Biol*. 18:638-642.

- Koonce, M.P. 1997. Identification of a microtubule-binding domain in a cytoplasmic dynein heavy chain. *J. Biol. Chem.* 272:19714-19718.

- Koonce, M.P., P.M. Grissom, and J.R. McIntosh. 1992. Dynein from Dictyostelium: primary structure comparisons between a cytoplasmic motor enzyme and flagellar dynein. *J. Cell Biol.* 119:1597-1604.
- Kwinter, D.M., K. Lo, P. Mafi, and M.A. Silverman. 2009. Dynactin regulates bidirectional transport of dense-core vesicles in the axon and dendrites of cultured hippocampal neurons. *Neuroscience*. 162:1001-1010.

- Lai, C., X. Lin, J. Chandran, H. Shim, W.J. Yang, and H. Cai. 2007. The G59S mutation in p150(glued) causes dysfunction of dynactin in mice. *J Neurosci*. 27:13982-13990.

- LaMonte, B.H., K.E. Wallace, B.A. Holloway, S.S. Shelly, J. Ascano, M. Tokito, T. Van Winkle, D.S. Howland, and E.L. Holzbaur. 2002. Disruption of dynein/dynactin inhibits axonal transport in motor neurons causing late-onset progressive degeneration. *Neuron*. 34:715-727.

- Levy, J.R., and E.L. Holzbaur. 2006. Cytoplasmic dynein/dynactin function and dysfunction in motor neurons. *Int J Dev Neurosci*. 24:103-111.

- Levy, J.R., and E.L. Holzbaur. 2008. Dynein drives nuclear rotation during forward progression of motile fibroblasts. *J Cell Sci*. 121:3187-3195.

- Lloyd, T.E., J. Machamer, K. O'Hara, J.H. Kim, S.E. Collins, M.Y. Wong, B. Sahin, W. Imlach, Y. Yang, E.S. Levitan, B.D. McCabe, and A.L. Kolodkin. 2012. The

p150(Glued) CAP-Gly domain regulates initiation of retrograde transport at synaptic termini. *Neuron*. 74:344-360.

- McKenney, R.J., M. Vershinin, A. Kunwar, R.B. Vallee, and S.P. Gross. 2010. LIS1 and NudE induce a persistent dynein force-producing state. *Cell*. 141:304-314.

- Mocz, G., and I.R. Gibbons. 1996. Phase partition analysis of nucleotide binding to axonemal dynein. *Biochem.* 35:9204-9211.

- Moughamian, A.J., and E.L. Holzbaur. 2012. Dynactin is required for transport initiation from the distal axon. *Neuron*. 74:331-343.

- Neuwald, A.F., L. Aravind, J.L. Spouge, and E.V. Koonin. 1999. AAA^{+}: a class of cheperone-like ATPases associated with the assembly, operation, and disassembly of protein complexes. *Genome Res.* 9:27-43.

- Ori-McKenney, K.M., J. Xu, S.P. Gross, and R.B. Vallee. 2010. A cytoplasmic dynein tail mutation impairs motor processivity. *Nat Cell Biol*. 12:1228-1234.

- Paschal, B.M., and R.B. Vallee. 1987. Retrograde transport by the microtubule-associated protein MAP 1C. *Nature*. 330:181-183.

- Pfarr, C.M., M. Coue, P.M. Grissom, T.S. Hays, M.E. Porter, and J.R. McIntosh. 1990. Cytoplasmic dynein localizes to kinetochores during mitosis. *Nature*. 345:263-265.

- Plamann, M., P.F. Minke, J.H. Tinsley, and K.S. Bruno. 1994. Cytoplasmic dynein and actin-related protein Arp1 are required for normal nuclear distribution in filamentous fungi. *J Cell Biol*. 127:139-149.

- Puls, I., C. Jonnakuty, B.H. LaMonte, E.L. Holzbaur, M. Tokito, E. Mann, M.K. Floeter, K. Bidus, D. Drayna, S.J. Oh, R.H. Brown, Jr., C.L. Ludlow, and K.H. Fischbeck. 2003. Mutant dynactin in motor neuron disease. *Nat Genet*. 33:455-456.

- Qi, Y., J.K. Wang, M. McMillian, and D.M. Chikaraishi. 1997. Characterization of a CNS cell line, CAD, in which morphological differentiation is initiated by serum deprivation. *J Neurosci*. 17:1217-1225.

- Quintyne, N.J., S.R. Gill, D.M. Eckley, C.L. Crego, D.A. Compton, and T.A. Schroer. 1999. Dynactin is required for microtubule anchoring at centrosomes. *J Cell Biol*. 147:321-334.

- Sakato, M., and S.M. King. 2004. Design and regulation of the AAA+ microtubule motor dynein. *J Struct Biol*. 146:58-71.

- Schroer, T.A. 2004. Dynactin. *Annu Rev Cell Dev Biol*. 20:759-779.

- Sivagurunathan, S., R.R. Schnittker, S. Nandini, M.D. Plamann, and S.J. King. 2012a. A mouse neurodegenerative dynein heavy chain mutation alters dynein motility and localization in Neurospora crassa. *Cytoskeleton (Hoboken)*. 69:613-624.

- Sivagurunathan, S., R.R. Schnittker, D.S. Razafsky, S. Nandini, M.D. Plamann, and S.J. King. 2012b. Analyses of Dynein Heavy Chain Mutations Reveal Complex Interactions between Dynein Motor Domains and Cellular Dynein Functions. *Genetics*.

- Smith, D.S., M. Niethammer, R. Ayala, Y. Zhou, M.J. Gambello, A. Wynshaw-Boris, and L.H. Tsai. 2000. Regulation of cytoplasmic dynein behaviour and microtubule organization by mammalian Lis1. *Nat. Cell Biol.* 2:767-775.

- Starr, D.A., B.C. Williams, T.S. Hays, and M.L. Goldberg. 1998. ZW10 helps recruit dynactin and dynein to the kinetochore. *J. Cell Biol.* 142:763-774.

- Suri, C., B.P. Fung, A.S. Tischler, and D.M. Chikaraishi. 1993. Catecholaminergic cell lines from the brain and adrenal glands of tyrosine hydroxylase-SV40 T antigen transgenic mice. *J Neurosci*. 13:1280-1291.
- Traer, C.J., A.C. Rutherford, K.J. Palmer, T. Wassmer, J. Oakley, N. Attar, J.G. Carlton, J. Kremerskothen, D.J. Stephens, and P.J. Cullen. 2007. SNX4 coordinates endosomal sorting of TfnR with dynein-mediated transport into the endocytic recycling compartment. *Nature Cell Biology*. 9:1370-U1355.

- Vissers, L.E., J. de Ligt, C. Gilissen, I. Janssen, M. Steehouwer, P. de Vries, B. van Lier, P. Arts, N. Wieskamp, M. del Rosario, B.W. van Bon, A. Hoischen, B.B. de Vries, H.G. Brunner, and J.A. Veltman. 2010. A de novo paradigm for mental retardation. *Nat Genet*. 42:1109-1112.

- Weedon, M.N., R. Hastings, R. Caswell, W. Xie, K. Paszkiewicz, T. Antoniadi, M. Williams, C. King, L. Greenhalgh, R. Newbury-Ecob, and S. Ellard. 2011. Exome sequencing identifies a DYNC1H1 mutation in a large pedigree with dominant axonal Charcot-Marie-Tooth disease. *Am J Hum Genet*. 89:308-312.

- Willemsen, M.H., L.E. Vissers, M.A. Willemsen, B.W. van Bon, T. Kroes, J. de Ligt, B.B. de Vries, J. Schoots, D. Lugtenberg, B.C. Hamel, H. van Bokhoven, H.G. Brunner, J.A. Veltman, and T. Kleefstra. 2012. Mutations in DYNC1H1 cause severe intellectual disability with neuronal migration defects. *J Med Genet*. 49:179-183.